2014

Magnetic Properties of Hematite (α-Fe2O3) Nanorods

Samar A. Ghopry
Virginia Commonwealth University, ghoprysa@vcu.edu

Magnetic Properties of Hematite (α-Fe_2O_3) Nanorods

Samar A Ghopry

Virginia Commonwealth University

Magnetic Properties of Hematite (α-Fe2O3) Nanorods

A thesis submitted in partial fulfillment of the requirements for the degree of Master of Science at Virginia Commonwealth University.

by

(Samar A Ghopry, B.S. in Physics Jazan University, 2007
M.S. in Physics/Applied Physics Virginia Commonwealth University, 2014)

Director: Dexian Ye, Assistant Professor, Department of Physics

Virginia Commonwealth University
Richmond, Virginia, 23284
December, 2014

Acknowledgments

First of all, I would like to thank my parents for raising us to love science. Since I was a kid, my father was telling me that I will be a scientist and my mother always has been sure that I will be successful at my study no matter how much difficulty I will have. Second I would like to thank the most amazing man in my life, my husband for believing in my. I want to thank him for all the sacrifices that he made for achieving my goal. I also would like to thank my kids for their patience and respects.

I also would like to thank the faculty members in the physics and chemistry departments at VCU who taught me classes that I need in order to satisfy the requirement to get my thesis. Furthermore, I would like to thank the teaching members of English language program and the international advisors for helping me linguistically to be able to study physics in the VCU. I would like to especially thank my graduate academic advisor, Dr. Dexian Ye for his assistance and for guiding me to achieve my goal. In addition I am thankful to Dr. Alison Baski, Dr. Ye and Dr. Michael Reshchikov for all of the supports that they provide to us in the meeting hour in the research and presentation skills. I would also like to thank Dr. Dimitry Pestov for helping me in the NCC.

Furthermore, I want to thank my friends at VCU Nahla Albarakati, Joy Mcnamara, Karen Phumisithiku, Ebtihaj Al Rashid, Lauren white, Turki al-Mugaiteeb and Dustin Clifford and outside VCU I want to thank Abdo Ojeeby and his family for all of the help they have given to my family and me. Finally I would like especially to thank Ibrahima Caseillo for all of his help and support.

Table of Contents

Figure list:

List of the tables:

Abstract

THE MAGNETIC PROPERTIES OF THE HEMATITE (α-Fe_2O_3) NANORODS

By Samar A Ghopry, Master of Science in Physics/Applied Physics

A thesis submitted in partial fulfillment of the requirements for the degree of Master of Science in Physics/Applied Physics at Virginia Commonwealth University.

Virginia Commonwealth University, 2014.

Major Director: Dexian Ye, Assistant Professor, Department of Physics

At this study three samples of hematite nanorods were deposited on the silicon substrates with different varieties of glancing angle deposition techniques. One sample (S1) was prepared by using thermal deposition with partially ionized beam (PIB) and substrate rotation. The second sample (S2) was synthesized by using thermal deposition with PIB and no substrate rotation. The third sample (S3) was obtained by using E-beam deposition, PIB and rotating substrate. In addition, one sample of magnetite nanorods (S4) has been prepared in order to compare the magnetic properties of the two different iron oxides. S4 was prepared by using thermal deposition and fixed glancing angle deposition, but no PIB was applied. The hysteresis loop has been studied for all samples

and the temperature dependent magnetic properties of one of the hematite samples and the magnetite been studied, too. The studies of the magnetic hysteresis for S1, S2, S3 and S4 showed that all of the samples have hysteresis loops but with dissimilar values of the saturation magnetization M_S, remanence M_R, and coercivity H_C. Furthermore, the hysteresis loops of all four samples showed different behaviors as the nanorods of the samples change the orientation with respect to the magnetic field. In addition to that fact, the hysteresis loop demonstrated that samples that have similar morphology have like behavior of the hysteresis loop. Also, it has found that S2 has the largest hysteresis loop of all hematite samples and it has large hysteresis loop in the perpendicular and parallel directions with the field as well. However, the magnetite hysteresis loops are significant larger than the ones of the hematite. Likewise, the studies of the temperature dependence magnetic properties of S2 and S4 showed that the ZFC and FC M-T curves of S1and S4 behaved differently when the direction of the nanorods changed from perpendicular to parallel with the field. In addition, the ZFC and FC M-T curves of hematite were different than the ZFC and FC M-T curves of magnetite.

Chapter 1: Introduction

Hematite, α-Fe_2O_3 is one of the iron oxides with the corundum crystal structure which has oxygen ions form a hexagonal close packed framework[1]. Hematite is an antiferromagnetic material at low temperature, which has zero net magnetic moment. However, it has some magnetic moment above a critical temperature called Morin transition temperature (T_M). Below Morin transition temperature, α-Fe_2O_3 is perfectly antiferromagnetic (AF) but it flips its magnetic phase above the Morin transition temperature and becomes a weak ferromagnetic material (WF) that has some net magnetic moment. This change of magnetic phase, which is called Morin transition and leads to the magnetic moments of α-Fe_2O_3, depends on the spin directions of the Fe^{3+} ions with specific c-planes[2]. The magnetic moments of the Fe^{3+} ions are ferromagnetic when the spin moments lie in the c-plane; however, when the spin moments change and become parallel to the c-axis the hematite becomes a perfect antiferromagnetic[3]. It has been found that T_M of the bulk hematite is 250K and both T_M and the spin flop transition field increase with increasing crystallite size of hematite[4]. Magnetic hysteresis loop is usually used to study the magnetic properties of hematite. It has been shown that hematite nanoparticles can have a hysteresis loop at room temperature, which depends on the size, shape, and crystallinity of the hematite nanoparticles.

Hematite is the most stable iron oxide and has n-type semiconductor properties under ambient conditions. These properties make it a very important martial for science and technology. Also, it is used as catalysts, magnetic material, pigments, gas sensors

and cathode in lithium-ion battery. The perfect level of the usage of hematite depends on the size of the particle since the size and the shape affect its properties such as the Morin transition. For example, by decreasing the size of the spherical nanoparticle of the hematite, T_M decreases.

At this study, the magnetic properties of the hematite prepared by different physical deposition methods have been investigated. Also, magnetite (Fe_3O_4) samples have been prepared in order to compare the magnetic properties of the two types of magnetic martials based on iron oxides. The hysteresis loops were studied for all of the samples and the magnetic moment vs temperature curves have been searched to understand the difference in the magnetic properties between the two materials.

1.1Magnetism

The physical phenomenon of magnetism covers magnetic fields and their effects upon materials. Magnetism has been known for thousands of years, but the principles and mechanisms that explain the magnetism phenomena are complicated and unclear until recently. Magnetic phenomena became very important in our life. Many of our modern technological devices depend on magnetism and magnetic materials such as electrical power generators and transformers, radios, televisions, telephones and computers. Iron and some steels are well-known examples of magnetic materials that exhibit magnetic properties.

Magnetic field can be generated using electric current or a magnet. Magnetic field that generated by moving electrically charged particles in a wire illustrated in figure 1.1.

The figure also illustrates the right-hand rule for determining the direction of the generated magnetic field. The red arrow indicates the direction of the current and the blue arrow shows the direction of the magnetic field. It is much easier to think of magnetic force in term of field and by drawing imaginary lines the direction of the force can be indicated.

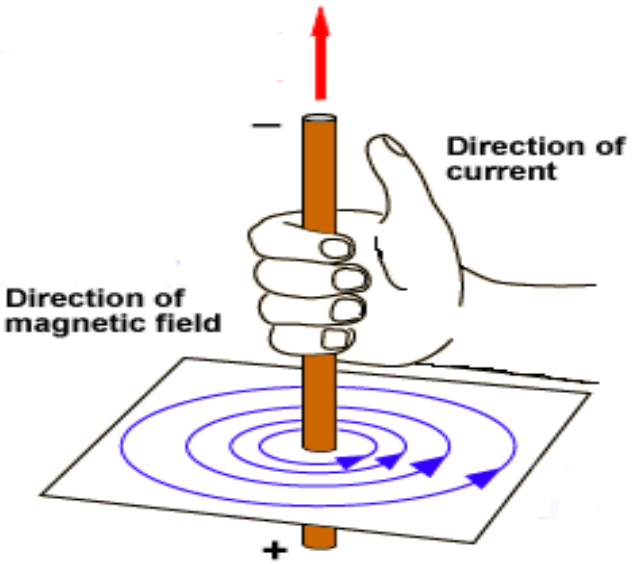

Figure 1. 1: Right-hand rule for electric wire

http://www.school-for-champions.com.

1.2 Magnetic dipoles:

Magnetic dipoles are found to take place in magnetic materials. Magnetic dipoles are similar to the electric dipoles in the dielectric material. However, a small bar of magnet may consist of north and south poles (magnetic dipoles) instead of positive and negative electric charges (electric dipoles), as shown in figure 1.2. Magnetic dipoles are influenced by magnetic fields. In a magnetic field, the magnetic force exerts a torque to

the magnetic dipole thus leads to orient the dipoles with the direction of the field. The figure shows the magnetic force between two different magnet bars. When the same poles of the magnetic bars face each other, repulsive force will be generated between them, figure 1.2 (a). When the opposite poles of the magnetic bars are next to each other, attractive force will be generated between them, figure 1.2 (b).

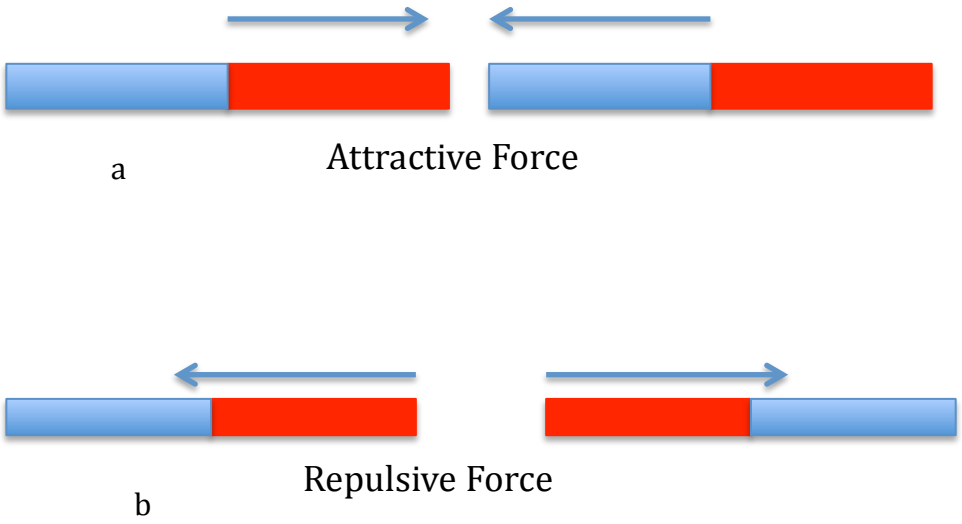

Figure 1.2: show the magnetic force between two different magnet bars a. show the attractive force between two magnetic bars facing by different magnetic poles b. show the repulsive magnetic force between two magnetic bars facing by same poles.

1.3 Magnetic field vectors:

Magnetic field can be generated by moving electric charge particles and can be calculated from Ampere's Law or the Biot-Savart Law with the unit of Amperes/meter (A/m). For example, if the generator of the magnetic field is a cylindrical coil (a solenoid) that consisting of N turns and with length L and carrying a current I, then the magnetic felid will be found from:

$$H = \frac{NI}{L} \quad (1.3.1)$$

The magnetic field *H* is generated by a cylindrical coil as in the figure 1.3 , and it shows that the current produces a stronger magnetic field inside the solenoid than outside since the field lines inside the solenoid are parallel and close to each other, and then the field is uniform in the strength and the direction. Therefore, the field that produced inside the coils behaves in a similar way to the ones of a bar magnet. From equation (1.3.1), magnetic field found to be increasing with the current (I) in the coil and with the number of the coil turn (N).

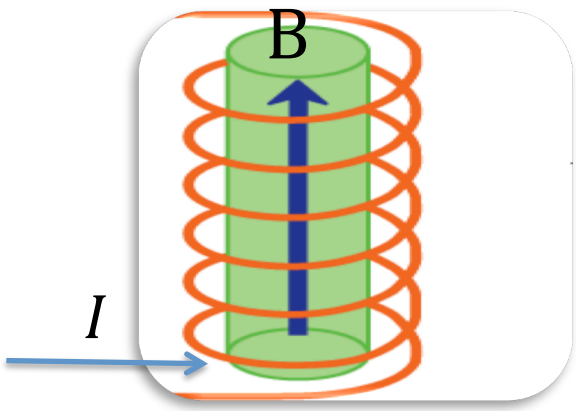

Figure 1.3: magnetic field generated by current in the solenoid.

bohr.winthrop.edu/.../courses/phys321/**Chap**%2020.pptx

1.4 Magnetic induction:

By subjecting a substance to a magnetic field *H*, the magnetic induction or the magnetic flux density (denoted by *B*) represents the magnitude of the internal field strength within a substance. The unit of *B* is Teslas [or Webers per square meter (Wb/m^2)]. Both *B* and *H* are vector fields, being characterized not only by magnitude, but also by direction in space.

The relationship between magnetic field strength and flux density according to;

$$B = \mu H \quad (1.4.1)$$

where the parameter μ is permeability, which is the property of the specific medium in which B measured when the *H* field passes through. The parameter μ has a unit of Webers per ampere-meter (Wb/A-m) or Henries per meter (H/m). In a vacuum the equation becomes:

$$B_0 = \mu_0 H \quad (1.4.2)$$

where μ_0 is the permeability of the vacuum, and it is the magnetic constant with value of $4\pi \times 10^{-7}$ (T m/A). The parameter B_0 is the flux density within a vacuum. The permeability of a medium μ can be known from the next equation

$$\mu_r = \frac{\mu}{\mu_0} \quad (1.4.3)$$

where μ_r is the relative permeability.

1.5 Magnetization:

Magnetization is the magnetic moment per volume with unit of (A/m),

$$M = \frac{m}{V} \quad (1.5.1)$$

where M is the magnetization, m is the magnetic moment and V is the volume. Magnetization and the magnetic field are related according to

$$M = X\,H \quad (1.5.2)$$

where X is the susceptibility. Equation (1.5.2) has shown that the magnetization of material relays on the susceptibility and how much is the strength of the magnetic field. Another equation that relates magnetic field to the magnetization is the expression:

$$B = \mu_0 H + \mu_0 M \quad (1.5.3)$$

1.6 Magnetic moment:

On atomic scale, a magnetic field can be induced by individual atoms since their electrons have a magnetic moment that they may get from the angular momentum. A magnetic moment occurs when a charged particle has an angular momentum. Originally, the magnetic moment comes from two sources that the orbital magnetic moment and the spin magnetic moment of each electron in the atom, figure1.4.

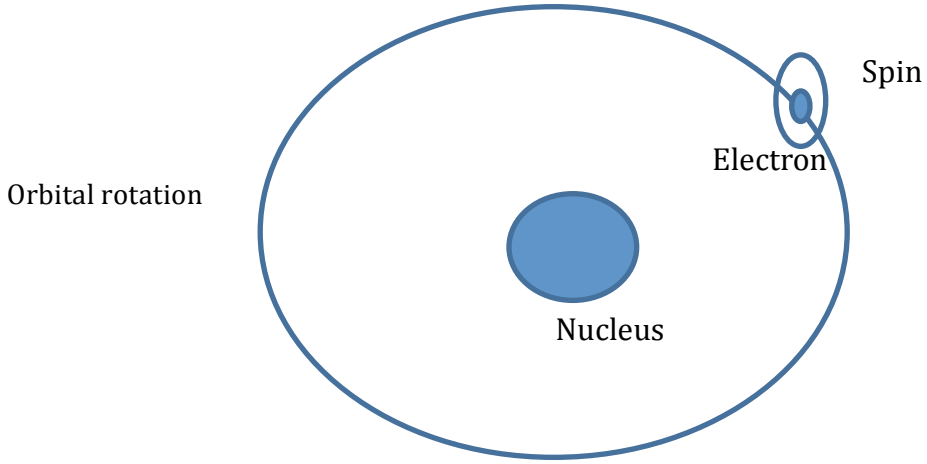

Figure: 1.4: Demonstration of the magnetic moment associated with an orbiting electron and a spinning electron.

In an atom, by orbiting around the nucleus continuously, electrons behave like a small current loop that generates a small magnetic field. In addition, by electron's spinning around its axis which are directed only in up or in down direction can lead to another magnetic moment. Also, the spin magnetic moment of the nucleus may increase the permanent magnetic moment. Therefore, the macroscopic magnetic properties of material are a result of the magnetic moments that caused by individual electrons and nuclei. The spin orientations in atoms control the magnetic properties of the material due to the imbalance of the spin and that depends on the number of the electrons in the atoms having paired or unpaired number of electrons. So when an atom has one electron in its outermost s-shell (unpaired), the electron aligns itself in an applied field then the magnetic will increase. So, in the solid state the magnetic moment of the atom is only due to its incomplete inner shell. However, atoms that have completely filled electron

shells or subshells have zero total magnetic moment as a result of the total cancellation of both orbital and spin moments when considering all electrons.

1.7 The classification of the magnetic materials:

1.7.1 Diamagnetic substances:

Diamagnetic material has very weak magnetization that is produced by electron motion. The orbital motion of electrons creates very small atomic current loops which lead to a tiny magnetic field. When an external magnetic field applied to the material, the current loops will align in such a direction in order to oppose the applied filed. Therefore, the diamagnetic material exhibits a negative magnetic susceptibility, as in figure 1.5. According to Lenz's law, the flow of an induced current is in such a direction as to oppose the change of flux of the induced field; this interprets the negative susceptibility. When the diamagnetic substances are placed between the poles of a strong electromagnet, they are attracted toward regions where the field is weak.

Diamagnetism is a property of all materials, but it can be observed only when other types of magnetism, paramagnetic or ferromagnetism, are totally absent since it is so weak. To satisfy the condition for pure diamagnetism, all electronic spins have to be paired and all orbital moments have to be either zero or effectively cancel one another.

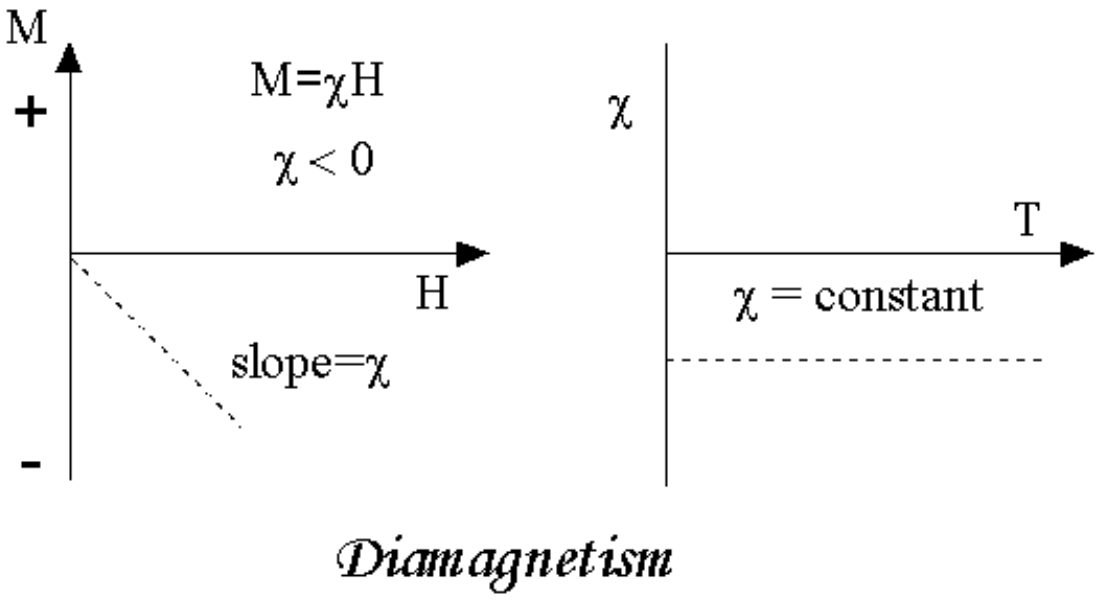

http://www.irm.umn.edu/hg2m/hg2m_b/hg2m_b.html

Figure 1.5: a negative magnetic susceptibility of The diamagnetic material.

1.7.2 Paramagnetism:

Paramagnetism is a magnetic property exhibited in material that can be magnetized just in the present of a magnetic field. When the paramagnetic material is positioned under a magnetic field, it will be magnetized parallel to the field, with permeability greater than 1 due to the incomplete cancellation of the magnetic moment as a result of the spin from unpaired electrons in atomic or molecular electron orbit constituent atoms or molecules. In the case of there is no external magnetic field applied, the orientations of these atomic magnetic moments are random, so the result is zero net magnetic moment, shown in figure 1.6. However, these atomic dipoles are free to rotate and do not interact with each other. Therefore, when a magnetic field is applied, the

dipoles align with the applied field as illustrated in figure 1.7, resulting in a net magnetic moment in the direction of the applied field and proportion to it.

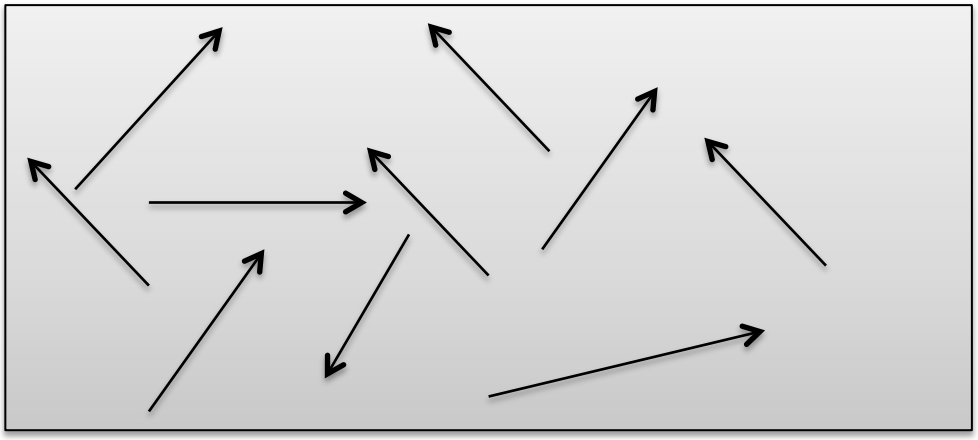

Figure 1.6: the orientation of atomic magnetic moments paramagnetic material at the absence of the magnetic field.

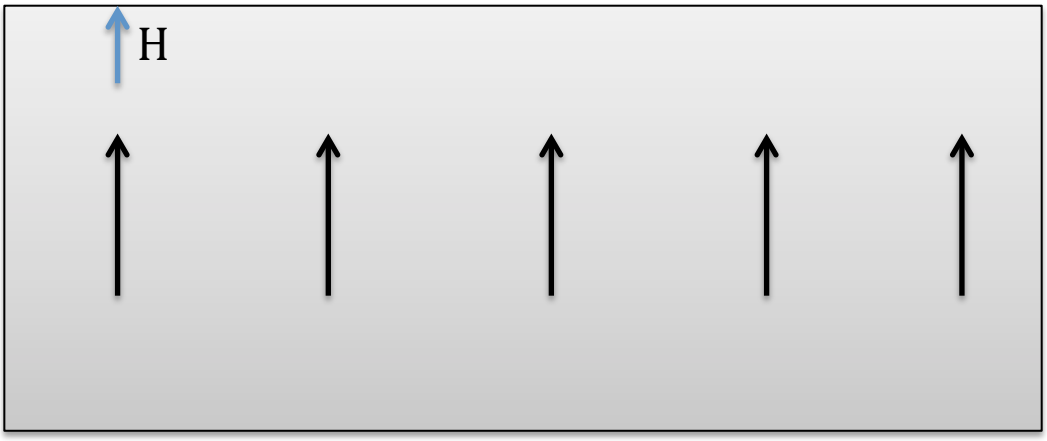

Figure 1.7: the orientation of the atomic magnetic moments of paramagnetic material under the effect of an applying field (H).

1.7.3 Ferromagnetism:

In the ferromagnetic material, there is a very strong interaction between the atomic moments that are produced by electronic exchange forces[5]. As a result of the very large exchange forces, parallel alignment of atomic magnetic moments can be obtained resulting in large net magnetization even there is no applied external magnetic field as in the figure 1.8 blow.

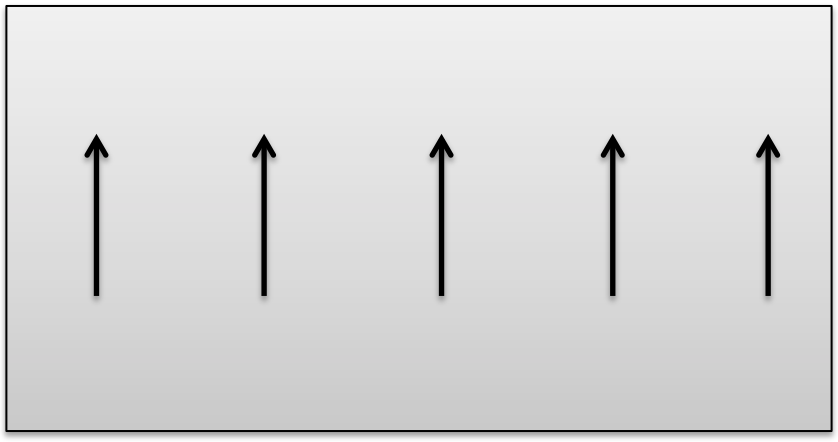

Figure 1.8: the direction of the atomic magnetic moments of the ferromagnetic material.

Ferromagnetic material has two distinguished characteristics. The first characteristic is the spontaneous magnetization which is the net magnetization of the substances at a zero magnetic field and it depends on the spin magnetic moments of electrons at zero temperature. Spontaneous magnetization is related to the saturation magnetization in term; however, the saturation magnetization is the maximum of the induced magnetic moment with an applied external magnetic field. In another words, the saturation magnetization is a point which the magnetization stops increasing while the magnetic field still rising, figure 1.9.

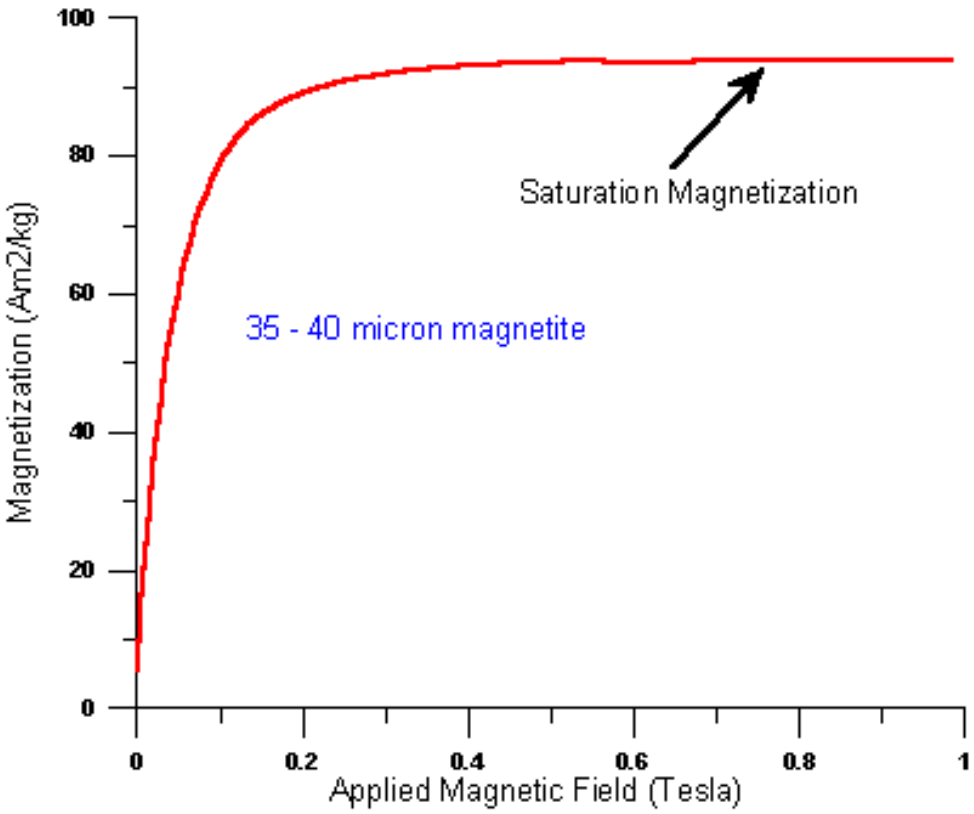

Figure 1.9: the saturation magnetization of ferromagnetic material.

http://www.irm.umn.edu/hg2m/hg2m_b/hg2m_b.html

The second distinguished characteristic is Curie temperature which indicates the change of the magnetic ordering. At **Curie** temperature, permanent magnetism materials flip to induce magnetism. Although the ferromagnetic materials have very large electronic exchange forces, this exchange can be overcome be thermal energy and result in a randomizing effect. Blow Curie temperature the ferromagnetism is ordered.

1.7.4 Ferrimagnetism:

Ferrimagnetic material has a more complex structure of magnetic ordering as a result of the crystal structure. The magnetic order of the ferrimagnetic material has population of atoms with two opposing magnetic sublattices as in the figure 1.10. Because the magnetic moments of the two sublattices are unequal, ferrimagnetism has a net magnetic moment. Therefore, it is similar to the ferromagnetism and exhibits the spontaneous magnetization, Curie temperatures, hysteresis, and remanence. Magnetite is an example of ferromagnetic material.

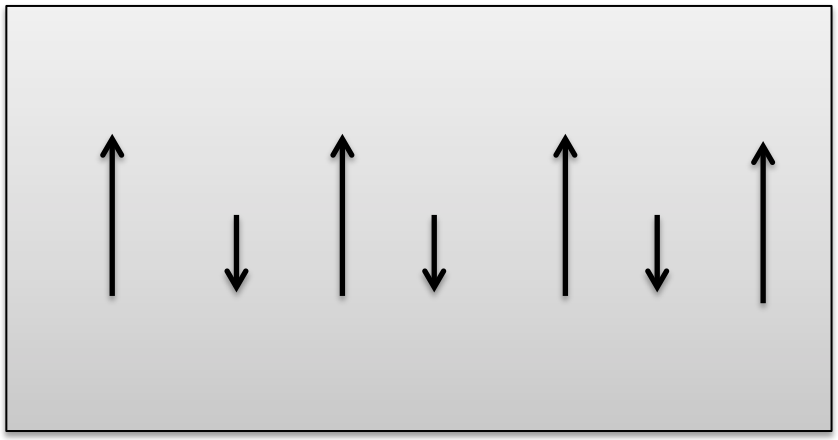

Figure 1.10: the atomic magnetic moments of the ferrimagnetic.

1.7.5 Antiferromagnetism:

In the antiferromagnetism, the two sublattice moments are exactly equal but in the opposite direction resulting in zero net magnetic moment, as shown in figure1.11. Antiferromagnetic material has a small positive susceptibility that changes with temperature since it behaves differently above a critical temperature which is the Neel temperature. With negative intercept, the susceptibility obeys the Curie Weiss law[6] of paramagnetic above Neel temperature[7]. Figure 1.12 shows the behavior of the susceptibility of antiferromagnetism above Neel temperature. However, antiferromagnetic material has no magnetic hysteresis loop and zero remanence, except for small deviations of ideal antiferromagnetism that is not exact anti-parallel. These deviations can produce a very small net magnetization since the spins between the neighbors are a bit tilted and they are called canted antiferromagnetism[8]. Hematite is one example of the canted antiferromagnetism.

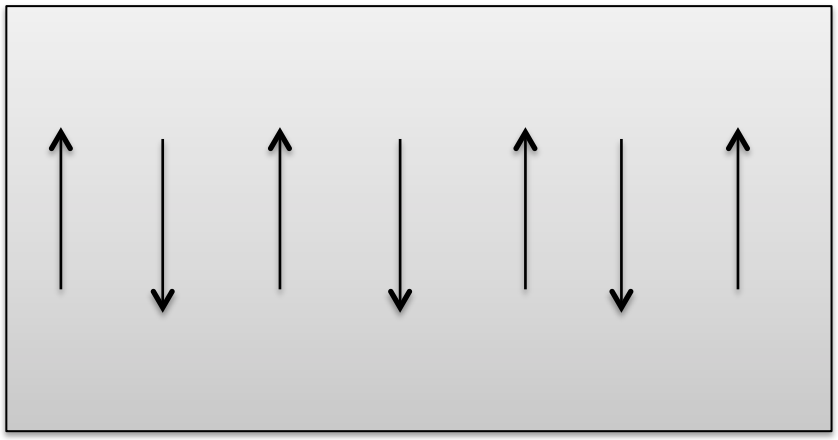

Figure1.11: the atomic magnetic moments of the antiferromagnetic material.

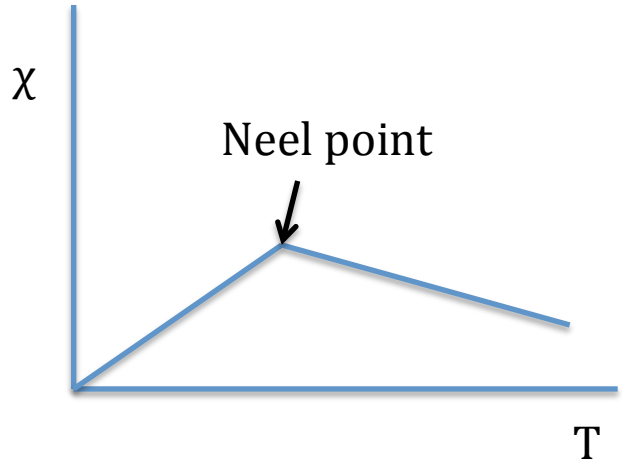

Figure 1.12: the behavior of the susceptibility of antiferromagnetism above Neel temperature.

1.7.5.1 Hematite:

The iron oxide of hematite that varies in form in color is one example of the antiferromagnetic material. It is a prefect antiferromagnetic material below T_M which is about 260 K and above the T_M hematite changes its magnetic phase to weak ferromagnetic material until the temperature get to Neel temperature. Neel temperature of hematite is 948 K. Above Neel temperature, hematite is paramagnetic.

The crystal structure of hematite is a corundum crystal structure with a hexagonal close packed framework of oxygen ions. The flip of the magnetic phase of the hematite occurred due to the direction of the magnetic spin of Fe^{3+} ions align to the specific c-plane. Above 263 K or -10 °C, the spin moments lie within c-plan, as the result a weak spontaneous magnetization will be produced and hematite becomes weak ferromagnetism. However, below 263 K or -10 °C, the spin moments become parallel to

c-plan and they will be canceled each other and the hematite become a perfect antiferromagnet as it illustrate in figure 1.13.

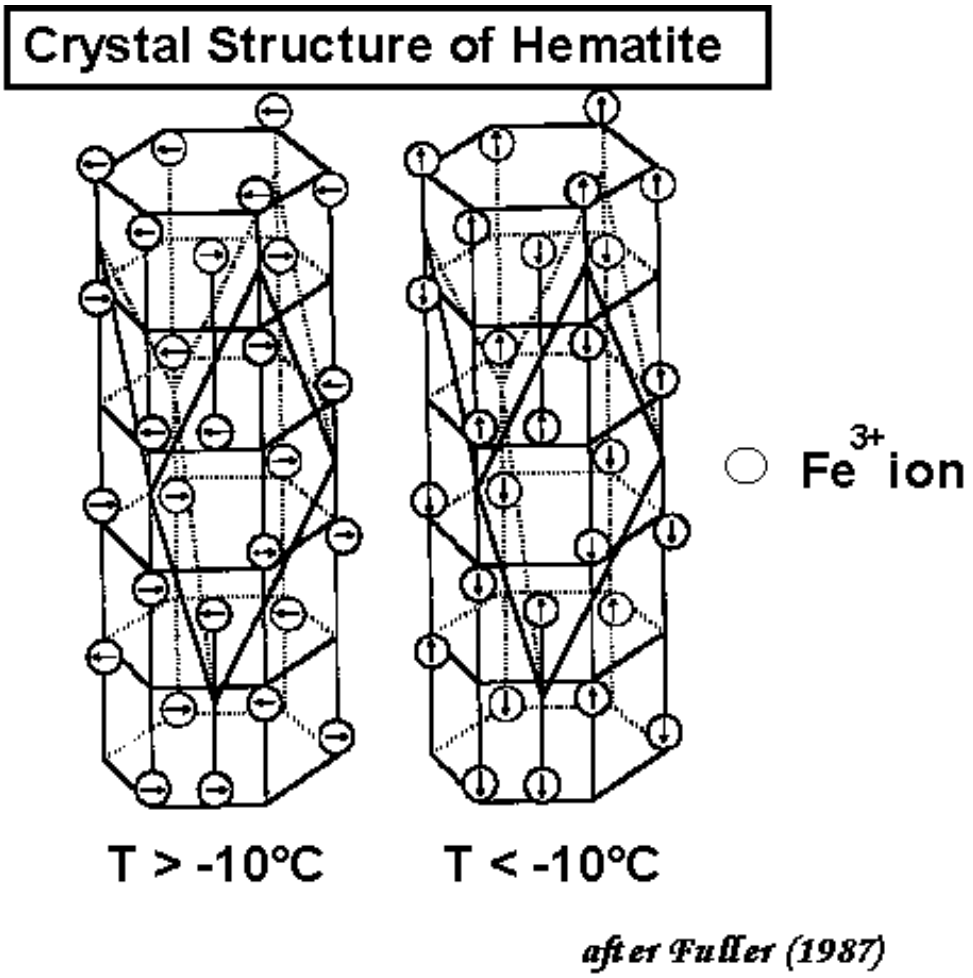

Figure 1.13: the different of the magnetic moment spin of antiferromagnetic material with the temperature.

Credit: http://www.irm.umn.edu/hg2m/hg2m_b/hg2m_b.html#top

1.8 Hysteresis loop:

When applying an external magnetic field to magnetic material, the magnetization of this material will response to the magnetic field through a loop called hysteresis loop[9]. For example, when ferromagnetic material such as iron, nickel or cobalt is subjected to an external magnetic field, it will not relax back to zero magnetization after the external field is removed. However, by applying a magnetic field in the opposite direction, it will be driven back to zero. The lack of traceability of the magnetization curve is the property called hysteresis and it is related to the existence of magnetic domains, i.e. magnetic ordering, in the material. This property of ferromagnetic materials is useful as a magnetic "memory". Permanent magnets will retain an imposed magnetization indefinitely.

1.8.1 Domains and Hysteresis Loop:

Ferromagnetic or ferrimagnetic materials are subdivided into small regions called domains by the magnetic ordering. The domains are separated by domain walls which are gradual reorientation of distinct moments across a limited area[10]. The width of the domain wall is determined by exchange and magnetocrystalline energies[11]. Figure 1.14 shows the effect of the exchange and magnetocrystalline energy on the width of the domain wall.

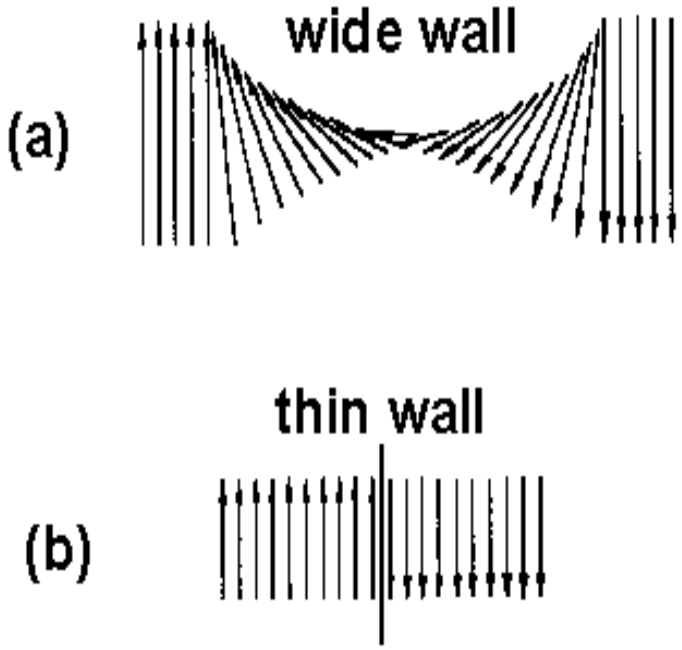

Figure 1.14: the 180° magnetization changes throw the domain wall

http://www.irm.umn.edu/hg2m/hg2m_d/hg2m_d.html

The figure above shows that the 180° magnetization changes through the domain wall and it could be (a) gradual or (b) abrupt and that depends on the exchange and anisotropy energies. The role of the exchanging energy is to keep spins parallel such that the total energy is a minimum. If the 180° rotation occurs gradually, the exchanging energy will remain small. However, since the spins through the wall cannot be aligned to an easy axis of magnetization any longer, the anisotropic energy is produced. The anisotropic energy is small in figure 1.14 (a) and low in figure 1.14 (b). So the exchange energy leads to enlarge the wall as wide as possible while the anisotropy energy leads to make the wall as thin as possible. Therefore, the domain wall has to maintain a finite width.

Grain could be consisted of more than one domain. In a single domain, all the magnetic dipole moments are aligned in the same orientation and each domain is spontaneously magnetized to saturation magnetization. However, because the directions of the magnetization are different from each other, the net magnetization of the entire solid is the sum of all the domains. The produced magnetization of the all domains of the ferromagnetic or ferrimagnetic material is near zero.

For ferromagnetic and ferrimagnetic material, the magnetic flux density B and magnetic field H are not linearly proportional to each other; instead B starts to vary as a function of H. Therefore, by applying magnetic field H, the B starts to increase slowly then fast with increased H, and at last becomes independent of H at high intensity of the magnetic field, as illustrated in figure 1.15. When the B reaches the maximum value, the saturated magnetic flux density B_S takes a place corresponding to the saturation magnetization M_S. The permeability will be determine from the sloop of B-H curve since the magnetic field strength and flux density are related by the equation blow:

$$B = \mu H \quad (1.8.1)$$

where $\boldsymbol{\mu}$ is the permeability.

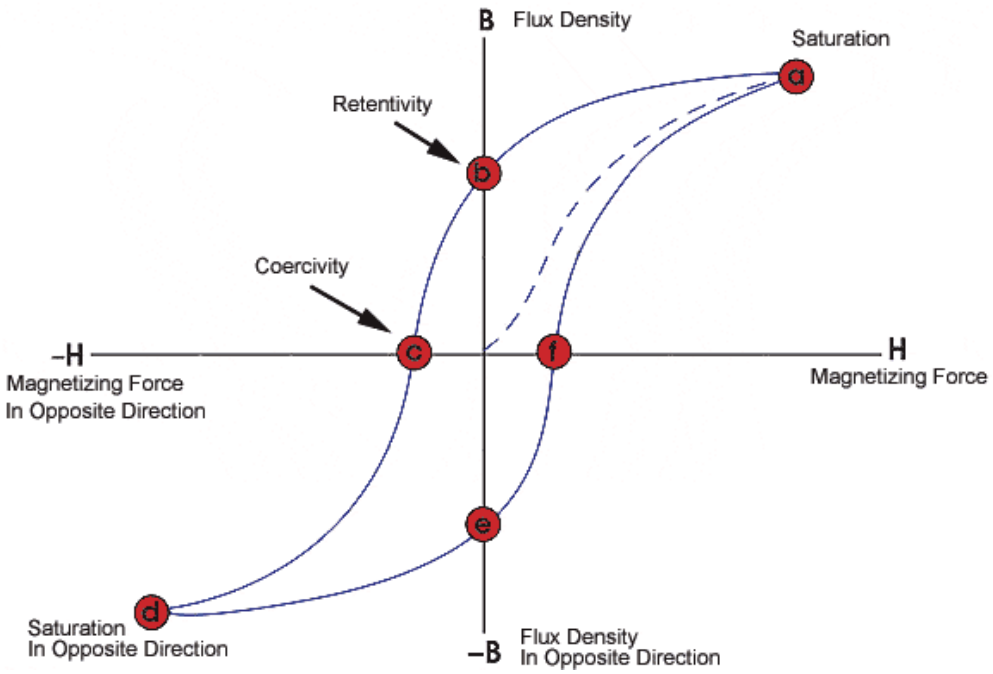

Figure 1.15: the hysteresis loop of ferromagnetic and ferrimagnetic.

Credit:

https://www.ndeed.org/EducationResources/CommunityCollege/MagParticle/Physics/HysteresisLoop.htm

Hysteresis loop behavior and permanent magnetization of the ferromagnetic and ferrimagnetic material may be explained by the movement of the domain walls as a result of being stressed under external magnetic field effect, figure 1.16. As the magnetic field applied, the shape and size of the domain walls change through the motion of domain boundaries. Initially, the magnetic moments of the constituent domains are oriented in random directions so that the net *B* (or *M*) field is zero. As the external magnetic field is applied, the domains will reorientate in the magnetic field direction. With increasing the field, the process of uniting the direction of the moment of the domain will continue until the macroscopic specimen becomes a single domain that is almost aligned with H. When the domain becomes perfectly aligned with the field saturation magnetization is achieved.

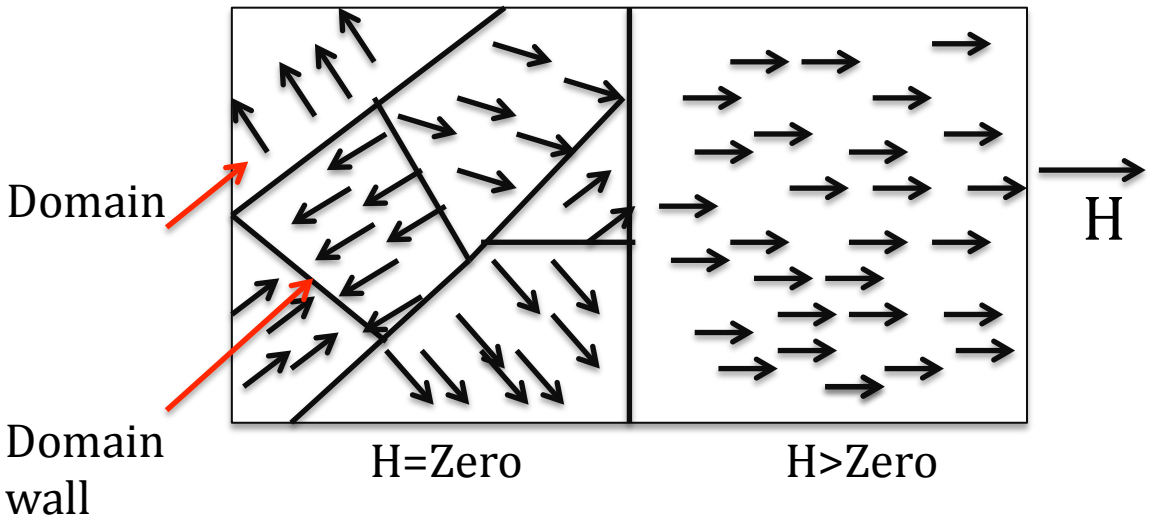

Figure 1.16: The effect of applying magnetic moment on the domains.

From saturation, as the magnetic field decreases by reversing the direction of the field, the magnetic flux density B or the magnetization will decease but in a very slow rate. As the field approaching zero, the magnetic flux density B or the magnetization does not reach zero, but persists as a remanence, remanent flux density B_R remanent magnetization M_R, or retentivity. So, the material stays magnetized even the absence of the external magnetic field H and that may be explained by the moving of domain walls. As reversing the field, the change of the domain structure reverses, too starting by the rotation of the magnetization of the single domain with the reversed field and then domains that with magnetic moment in the direction of the new magnetic field will form and grow against the former domains. As a response of the increase of the magnetic field increasing the field in the opposite direction, resistance to movement of domain walls takes a place and that explains the lag of magnetic flux density with magnetic field. When

H goes to zero, there is still some domains that has magnetic moment in the former direction resulting in the remanence B_R.

In order to reduce the magnetic flux density or the magnetization M within the specimen to zero, applied field must increase in the opposite direction corresponding to the **coercivity (**H_C*)*. As the field increases further in the opposite direction, it results in the saturation of the magnetization M but in the opposite direction. As the field does the second reversal to the point of the initial saturation, symmetrical hysteresis loop completes.

The Magnetic hysteresis does not take the same behavior for all the magnetic materials and depends on the class of magnetic material. For example, the magnetic hysteresis of ferromagnetic/ferrimagnetic materials is different from the ones of paramagnetic and diamagnetic. Figure 1.17 shows the difference between the linear magnetic hysteresis of the magnetic materials such as the paramagnetic and diamagnetic materials and the nonlinearity of most of the ferromagnetic/ferrimagnetic.

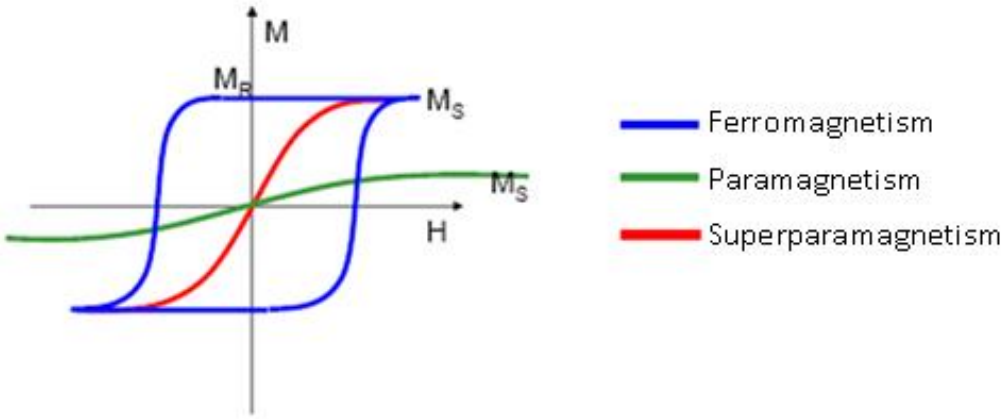

Figure 1.17. The different between the magnetic hysteresis of the magnetic material

http://www.science20.com/mei/blog/blocking_temperature

Chapter 2: Motivation and Literature Review

Understanding the magnetic properties of iron oxide nanomaterials has been a long-term goal for scientists and engineers. Studies showed that the magnetic properties are dependent on the size, surface state and the shape of the iron oxide at nanoscales. It has been shown that the Morin temperature (T_M) of hematite increases with increasing the spherical particle size. For example, the size effect of the α-Fe_2O_3 nanorods on the T_M has been studied using the temperature dependent magnetization curves under zero-field-cooled (ZFC) and field-cooled (FC) conditions. ZFC and FC from 4 to 300 K with 500 Oe applying field have been applied to study three different sizes of nanorods. The T_M of 60-90 nm nanorods with porosities of 20-50 nm is 255 K and with decreasing the diameter of the nanorod the TM decreases until it disappears with a size less than 15nm[12].

Hysteresis loop of magnetic material also has been affected by the size and shape. The investigation of shape anisotropy effect on the magnetic properties of hematite has been studied. Uniform nanocubes of hematite with an average size of 15 nm have been synthesized by hydrothermal method. The superconducting quantum interface device (SQUID) magnetometer (Quantum Design MPMS XL) has been used to study the magnetic properties of those samples. From 10 to 300 K and under an applied magnetic field of 100 Oe, the temperature-dependent magnetization was studied using ZFC and FC procedures. This study showed that, at an external field of 100 Oe, the blocking temperature (T_B) of hematite nanocubes is at 80 K[13].

By using the hydrothermal method again hematite nanomaterials were prepared, but in plate-like morphology with width ~ 500 nm and thickness ~ 100 nm, and then magnetic properties of the sample were studied. The hysteretic loop behavior of the samples showed that the material is in the weak ferromagnetic state at room temperature with the coercivity, remanent magnetization and saturation magnetization are H_C = 1140 Oe, M_R = 0.125 emu/g and M_S = 2.15 emu/g, respectively. However, at 5 K the hysteretic loop exhibited in a behavior of anti-ferromagnetism which has a small hysteresis loop with the remanent magnetization M_r = 0.0027 emu/g and coercivity H_C = 150 Oe. Moreover, the Morin temperature was studied and it was observed at $T_M \approx 250$ K[14].

Also, the magnetic properties of α-Fe_2O_3 nanowires prepared by oxidizing pure iron are studied. From 4 to 200 K and under an applied field of 100 Oe, the temperature dependence of the ZFC and FC magnetization ware investigated. It has been shown that the blocking temperature of the α-Fe_2O_3 single-crystal nanowires is 120 K and no obvious evidence of Morin transition, and the hysteresis loops was varied with temperatures[15].

Magnetite (Fe_3O_4) is another magnetic material that its magnetic properties can be affected by the size, shape and crystal structure. Magnetite hollow spheres with five different diameters were prepared by changing polyvinyalpyrrollidon (PVP)[16]. By using FC and ZFC procedures, magnetic properties have been studied for the different samples in a temperature range of 80 K and 300 K. The FC and ZFC curves of all the samples showed split at 300 K; so, all the samples are ferromagnetic within the temperature range of 80 K and 300 K with blocking temperature that could be at or above 300 K. In

addition, magnetization of all samples are increasing and creating a cusp around a certain temperature (T_V), which is called Verwey transition temperature. Magnetization increased in the same samples and remained constant for other samples after Verwey transition. The T_V of all samples were size dependence since it decreases with decreasing sphere diameter and it was close to the bulk value for the largest sphere at a diameter of 725 nm. Furthermore, the Day plots were used in this study to give an insight of domain structure of the samples. It showed that with increasing the size the domain structure flips from pseudo single domain (PSD) to multi domain (MD) structure, but the samples with smaller spheres exhibits only the SD type of domain structure at lower temperatures. Also, the hysteresis loops were studied for all the samples. It showed that the samples with smaller diameters have higher remanence magnetization (M_R); however, they have low a saturation magnetization (M_S) when compared to samples with bigger sizes[17]. Furthermore, by using the sol–gel method and annealing under vacuum, Fe_3O_4 nanoparticles have been prepared at different temperatures at 200, 250 and 400 ^oC. The hysteresis loops of the Fe_3O_4 nanoparticles at room temperature are shown that the saturated magnetization value and the coercivity increase continuously with increasing annealing temperature in the temperature range studied[18].

Monodispersed faceted and cubic magnetite nanoparticles were synthesized by the reduction of iron (III) acetylacetonate ($Fe(acac)_3$) with N-methylpyrrole or pyrrole in the presence of the surfactants oleic acid and oleylamine in air. Hysteresis loops of different sizes of magnetite nanoparticles have been studied. It showed that the effect of

the sizes of the Fe_3O_4 nanoparticles is distinct. It is found that the 3.2 nm magnetite nanoparticles are superparamagnetic, but when magnetite nanoparticles have a larger size, they become ferromagnetic. Also, the magnetization-temperature dependent curves for FC and ZFC of Fe_3O_4 nanoparticles under an applied magnetic field of 1000 Oe have been investigated. The T_B of samples are different for different sizes. The T_B is around 25 K for the 3.2 nm magnetite nanoparticles; however, when the particle size increase to 5.4 and 10.3 nm, the T_B rise to 330 and 360 K, respectively[19].

Furthermore, iron oxide's magnetic properties can be modified due to the methods of synthesis. Two samples of hematite nanorod were prepared by an iron-water vapor reaction (sample 1) and hydrothermal methods (sample 2), to study the magnetic properties of hematite nanoparticles. SQUID magnetometer was used to obtain the hysteresis loop and the Morin transition temperature of the two samples. The hysteresis loops of the two samples showed unlike magnetic domain type behaviors. An MD-type behavior (MR/MS = 0.06) was observed in sample 1 of the hematite nanorods, but sample 2 of the hematite was showing a PSD-type behavior (MR/MS = 0.28). The Morin transition of sample 1 was observed at 122 K under an applied field of 100 Oe. However, there was surprised behavior under an applied field of 10 Oe which is unexpected decreasing of magnetic susceptibility at ca. 122 K. However, sample 2 of the hematite shows only weak curvature in the ZFC curves and there were no obvious Morin transition[20].

All the studies surveyed above are focused on nanoparticles prepared by different deposition techniques. Anisotropic magnetic properties are rarely reported due to the simple and isotropic geometry of the nanoparticles. At this study, the magnetic properties

of the hematite nanorod arrays that have been prepared by different physical deposition have been investigated. Also, a sample of magnetite nanorods has been prepared in order to compare the magnetic properties of the two magnetic materials. The hysteresis loops were studied for all of the samples and the temperature dependent magnetic moment has been searched for just one sample of the hematite and the sample of the magnetite to understand the difference in the magnetic properties between the two materials.

Chapter 3: Experimental Setup

The process of the deposition requested three different techniques of the deposition that started by evaporating the source with and without partially ionization of the vapor to enhance the growth of iron oxide nanorods using glancing angle deposition technique.

3.1 Experimental setup for samples S1 and S2

The same process was used to prepare samples S1 and S2 with one difference. The process will be explained in detail.

3.1.1 Thermal deposition

The samples were deposited onto silicon (100) substrate by using a homemade thermal depositor with partial ionization beam. Chamber is shown and labeled in figure 3.1. A mechanical scroll pump and a turbo molecular pump were used to achieve the required low pressures to grow the samples. The base pressure in the chamber was around $5x10^{-7}$ Torr. An ionization pressure gauge was used to measure the base pressure. In an ion gauge, adjusted electron currents are produced by heating a filament and then a positive voltage is applied to a helical grid to catch the electron current. When the electrons move to the grid, some of them collide with gas molecules as a result they will be ionized. Because of the applied negative voltage of the central collector, these ionized molecules are attracted to it. The pressure in the chamber is related to the current of the

ions.

In this thermal evaporation system, the source is evaporated from a graphite crucible. A tungsten filament surrounding the crucible is used to emit thermoelectrons. Then, by applying a voltage bias up to 1000V between the filament and the crucible, the thermoelectron current is directed towards the crucible. The bombardment of electrons onto the outer wall of the crucible heats it to the required temperature.

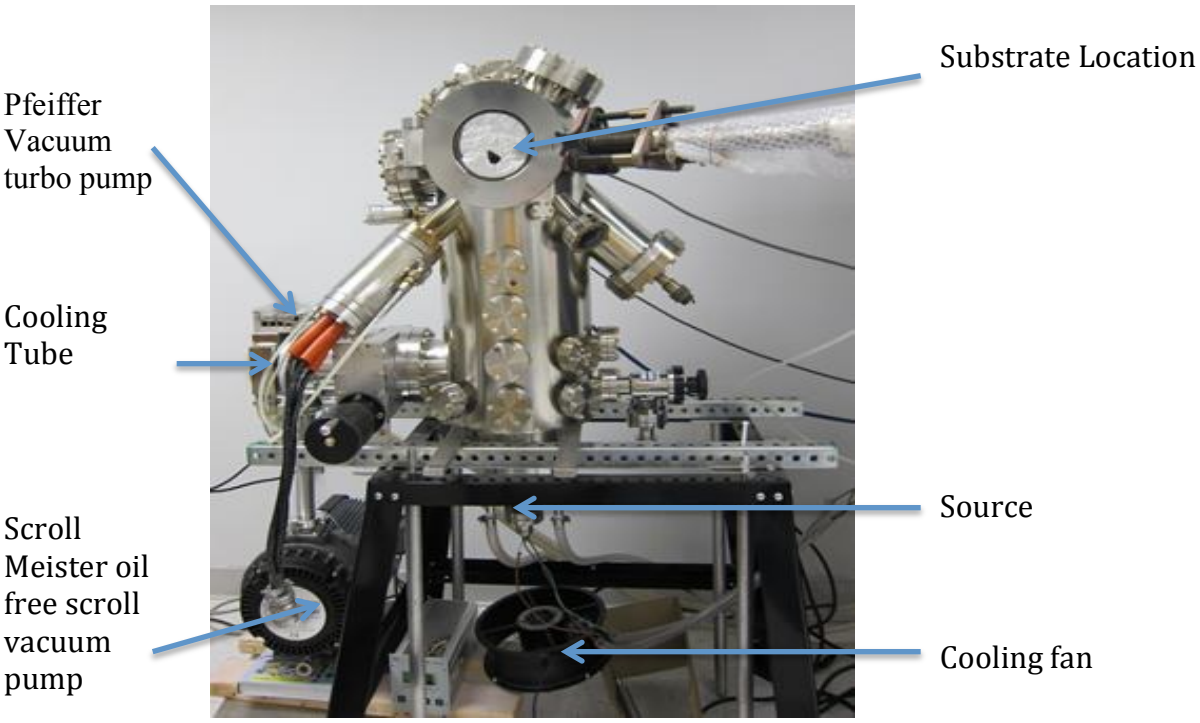

Figure 3.1: the homemade chamber of thermal deposition.

3.1.2 Partially ionized beam (PIB)

During the experiment, partially ionized atoms are self-generated by the bombardment of the accelerated electrons onto evaporated atoms from the crucible. The

ions then pass through another electric field above the crucible to gain kinetic energy up to 3.5 KeV. This partially ionized beam deposition (PID) can promote the growth of the crystalline structure on the substrate[21 22]. During growth, the overhanging atoms on the substrate can be removed by the energetic ions from the deposition vapor. In addition, the mobility and chemical reactivity are thermally enhanced as a result of the atomic collisions between incoming ions and deposited atoms. So, adding ionized, atoms to the deposition system produces high quality deposited nanomaterial since it improves surface diffusion, local heating, collapse of voids and recrystallization[23].

3.1.3 Glancing angle deposition (GLAD)

By combining a tilted substrate and substrate rotation to the system as in the Figure 3.2, two samples of the hematite were prepared. Sample S1 and sample S2 were grown on silicon substrates by using glancing angle deposition technique at a large oblique angle (85°) between the substrate and the incident flux, figure 3.2[24 25 26]. The deposition angle is determined by measuring the angle between the substrate normal and the direction of the incident vapor flux. The substrate can be set to rotate about its axis by a computer controlled stepping motor. Two different areas of height obtain due to the shadowing effect as a result of the oblique angle deposition at 85° deposition angle, as shown in figure 3.3. The lower areas will be shadowed by the taller areas of the film and then the nanorods in the shadowed area will stop growing because the impinging atoms will be blocked. As the taller areas continue to collect atoms, porous columnar microstructure of isolated grains keep growing along its axial directions until they are shadowed; as a result, the taller initial areas grow into nanorods.

Samples S1and S2 of hematite nanorods were grown on a silicon substrate at an oblique angle α ~85°. The difference between the two samples is that the substrate of the S1 was rotated about its axis and the S2 was set to be fixed.

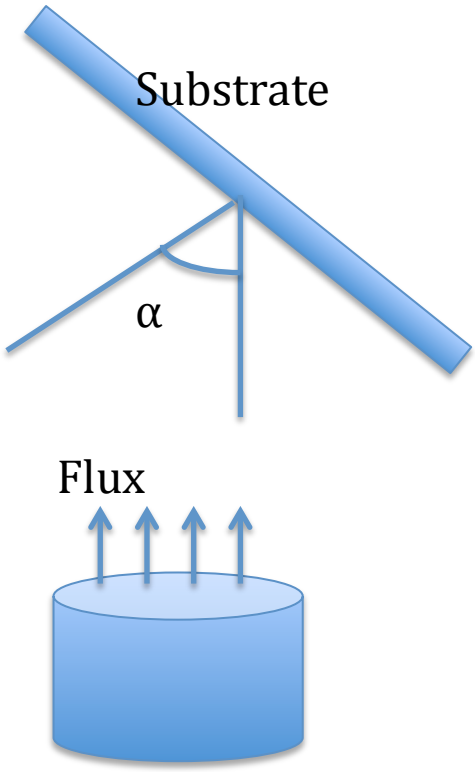

Figure 3.2: Diagram of oblique angle deposition.

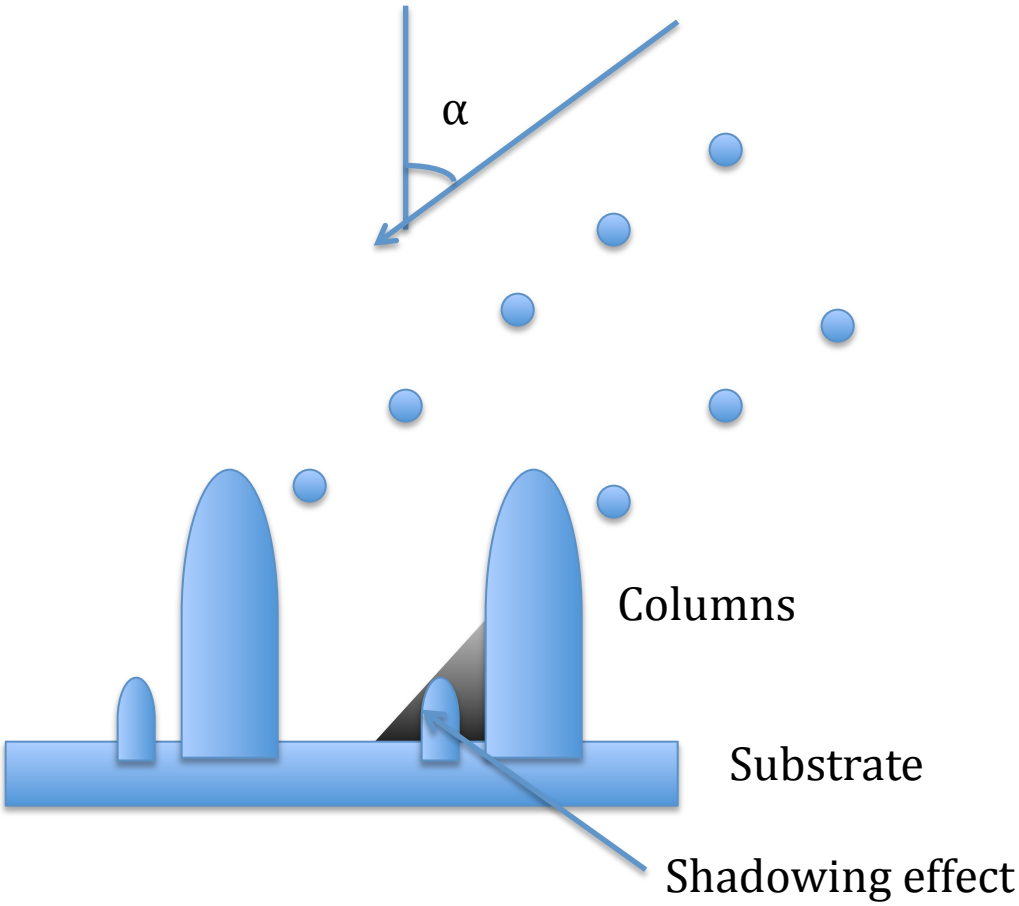

Figure 3.3: The effects of shadowing throw glancing angle deposition.

3.2 Experimental setup for sample S3

The deposition of sample S3 was carried out in the electron beam deposition system with the glancing angle deposition setup. The substrate was rotated and self-generated partially ionized beam was included to promote the growth of the nanorod,

Sample S3 was deposited onto a silicon substrate by using a factory made electron beam physical vapor deposition system. The base pressure in the deposition chamber was achieved by a molecular turbo pump to at least 7.5 x 10^{-5} Torr. Under high vacuum, a charged tungsten filament can generate an electron beam as in the figure 3.4. A 10 KV voltage was applied to accelerate the generated electron beam to a high kinetic energy and a set of magnets was used to direct the energetic beam towards the crucible to evaporate material. Simultaneously, source small portion of the evaporated atoms can be ionized by the energetic electron beam. This part of ions was accelerated by an additional DC bias that was connected to the chamber to help the growth of the material on the rotating glancing angle substrate, see Sections 3.1.2 and 3.1.2

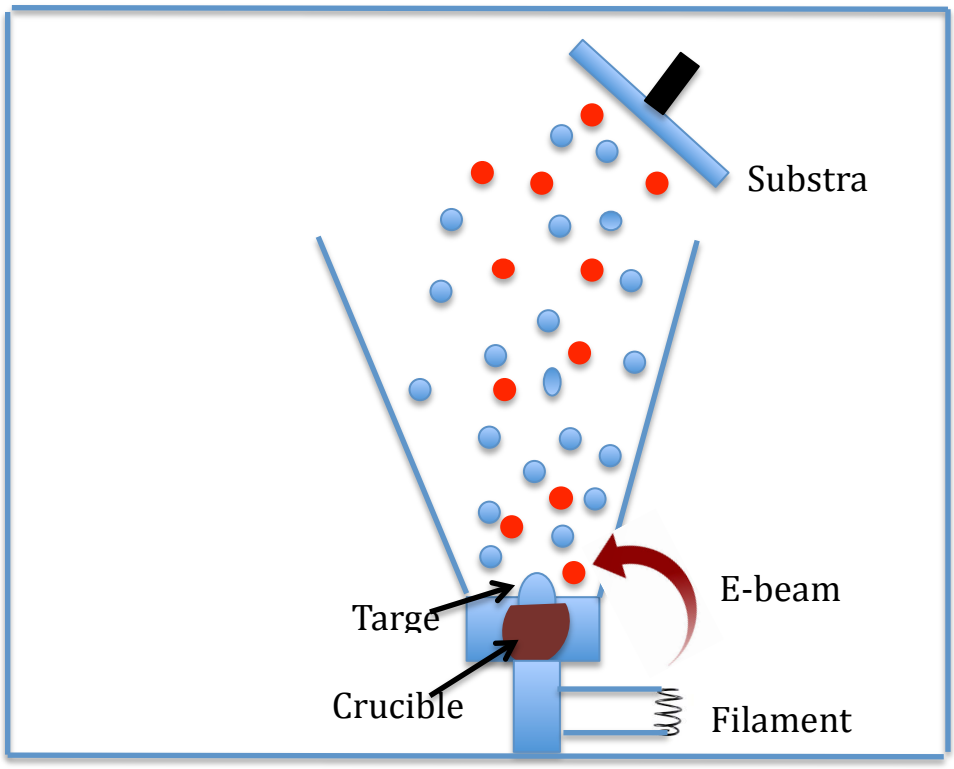

Figure 3.4: Experimental setup of sample S3.

3.3 Experimental setup for sample S4

In case of sample S4, the deposition material has been changed to Fe_3O_4. Instead of deposit hematite as in S1, S2 and S3, magnetite was deposited on fixed GLAD and no partially ionized beam was applied for this sample.

The table blow shows the differences between the Experimental Setup of samples.

Sample	Experiment setup
S1	Hematite, Thermal deposition, Ion beam assisted (IBA), Rotating Substrate.
S2	Hematite, Thermal deposition, Ion beam assisted (IBA), Fixed Substrate.
S3	Hematite, E beam deposition, Ion beam assisted (IBA), Rotating Substrate.
S4	Magnetite, Thermal deposition, no Ion beam assisted (IBA), Fixed Substrate.

Table 3.1: The experimental setup of S1, S2, S3, and S4.

Chapter 4: Characterization

4.1 X-ray diffraction (XRD)

X-Ray Diffraction (XRD) pattern is used to study the crystal structure of the prepared samples. X-ray Diffraction is a tool to determine the order of the atoms in a crystal by using X-ray. As the X-rays hit a crystal, they are diffracted into many directions. By detecting the angle and the intensities of the diffracted beams, the position of the atoms in the crystal lattice can be known.

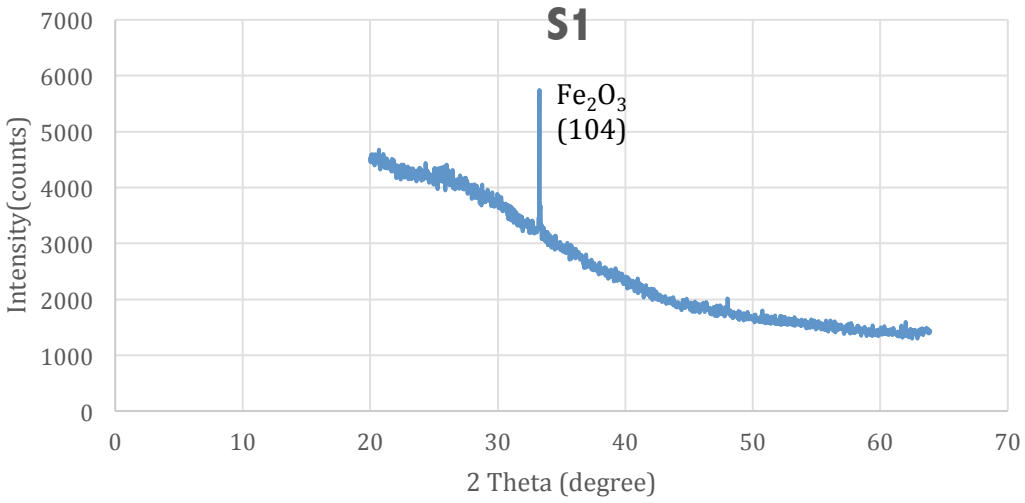

Figure 4.1: XRD pattern of sample S1

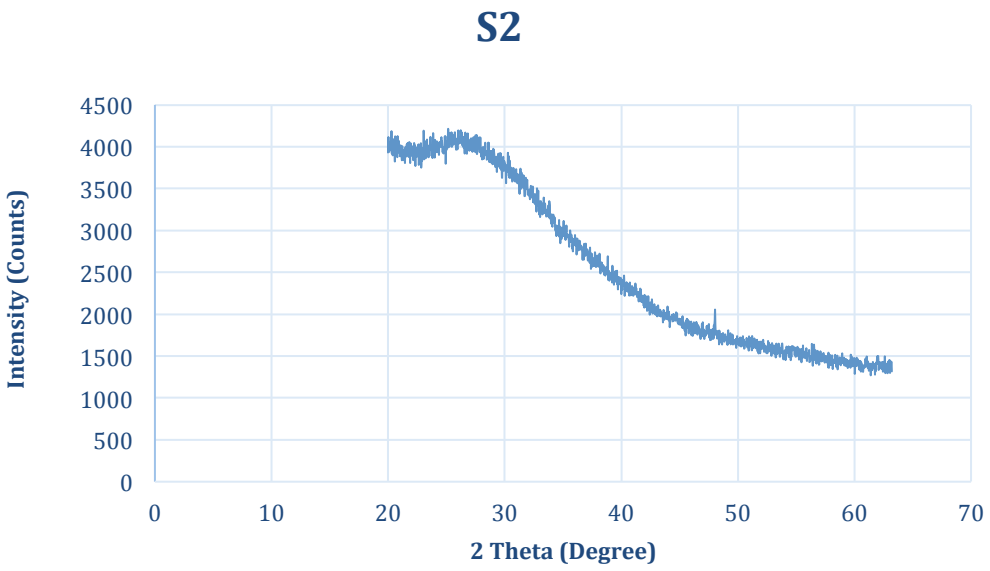

Figure 4.2: XRD pattern of S2

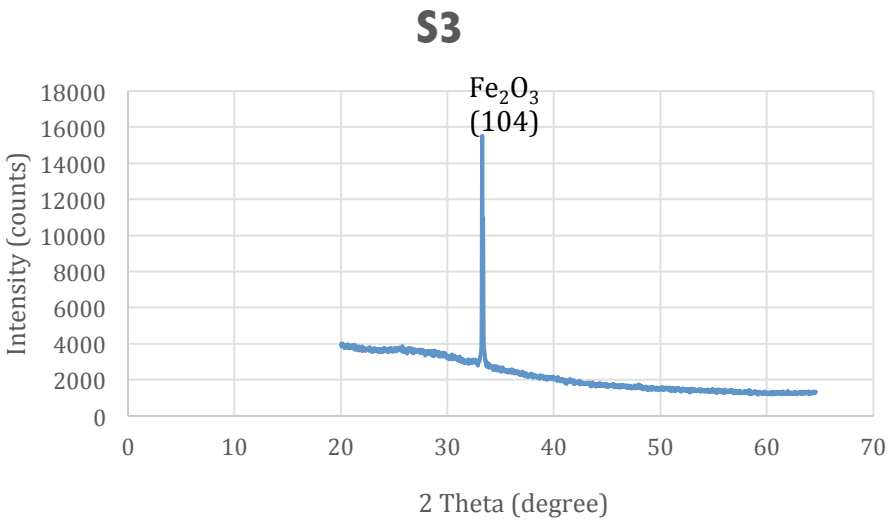

Figure 4.3: XRD pattern of S3

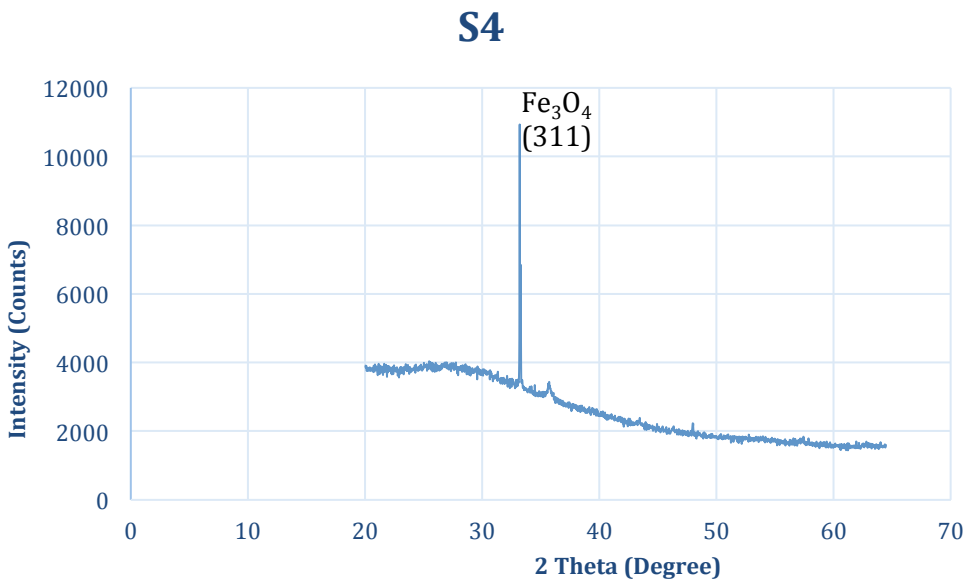

Figure 4.4: XRD pattern of S4

The crystal structure of the nanorods was examined by XRD. Figures 4.1, 4.2, 4.3 and 4.4 are showing the XRD patterns of the samples S1, S2, S3 and S4. The 2θ angle collection ranges from 20° to 65° with a scan rate of 2° per minute. Figures 4.1 and 4.3 show the XRD patterns of samples S1 and S3 of hematite nanorods, which are single crystalline with (104) orientation along the nanorod axis. According to JCPDS file no. 84-0307, the peaks of the S1and S2 hematite nanorods are assigned to (104) direction. The peaks of S2 almost disappeared as showing in the figure 4.2, indicating a noncrystalline nature of the sample. Figure 4.4 shows the single crystalline of the magnetite nanorods with a peak at the (311) direction according to the crystal database (ICDD, Ref. No. 00–003–0862).

4.2 SEM imaging

The samples were characterized using scanning electron microscope (SEM). A SEM uses a beam of electrons to obtain information about sample's morphology and composition. The schematic of the SEM is shown in figure 4.5. The field emission electron beam with energy from 0.2 KeV to 40 KeV is focused to the center by one or two condenser lenses to a size about 0.4 nm to 5 nm in diameter. The electron beam passes through scanning coils pairs of deflector plates to deflect the beam in two axes, X and Y. The scanning is over a rectangular area of the specimen surface in a raster fashion. As a result of the exchanging energy between the electron beam and the sample, secondary electrons are generated from the surface of the sample which can be detected and used to create the images of the sample.

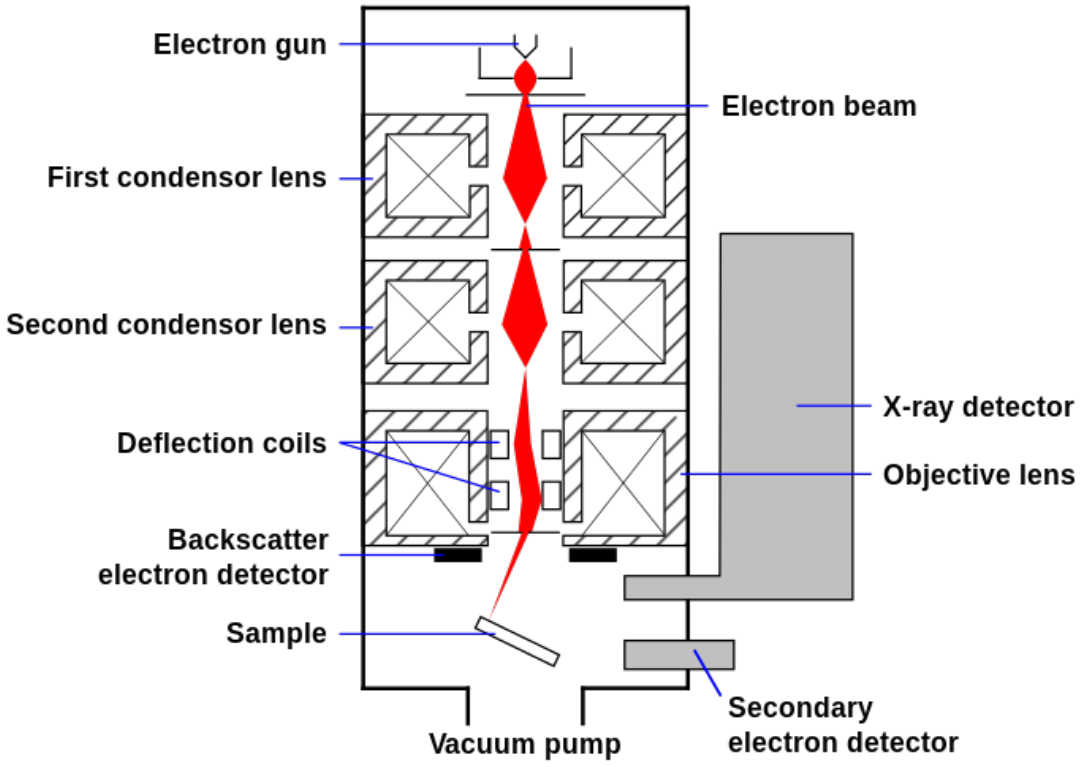

Figure 4.5: Schematic of an SEM

(Credit: Wikipedia)

The SEM images of all the samples in both top view and cross sectional view were taken in the Hitachi SU-70 SEM with a 5 KV acceleration voltage applied to the electron beam. Figure 4.6, 4.7 and 4.8 show the SEM images of the S1, S2 and S3 of the hematite in order, and the figure.4.9 displays the SEM images of the S4 of the magnetite. All the images indicate that the shape of all samples is nanorod with some difference in the size and the degree of the uniformity.

It is shown in figures 4.6 (b) and (d), the appearance of S1 is the hematite nanorod with

the diameter ranging from 30 to 50 nm. From figure 4.7 (d), it can be seen that the diameter of nanorod of the S2 is less than 20 nm. The diameter of the nanorod of the S3 is about 30 nm. However, the figure 4.9 shows that the nanorod of magnetite has the largest diameter that is measured to be about 100 nm. In addition, from the SEM images above, it is very clear that the deposition conditions on the rotating glancing angle substrate affected the growth of nanorods. The images of S1 and S3 that were deposited on the rotating substrate demonstrate that the nanorods were grown vertically along the normal of the substrate. In the other hand, the images of S2 and S4, which has been deposited on the fixed substrates, showed that the nanorods were grown in a titled angle to the substrate. In addition, the images of S3 shows that the morphology is much more uniform comparing to the one we prepared by using thermal deposition, S1.

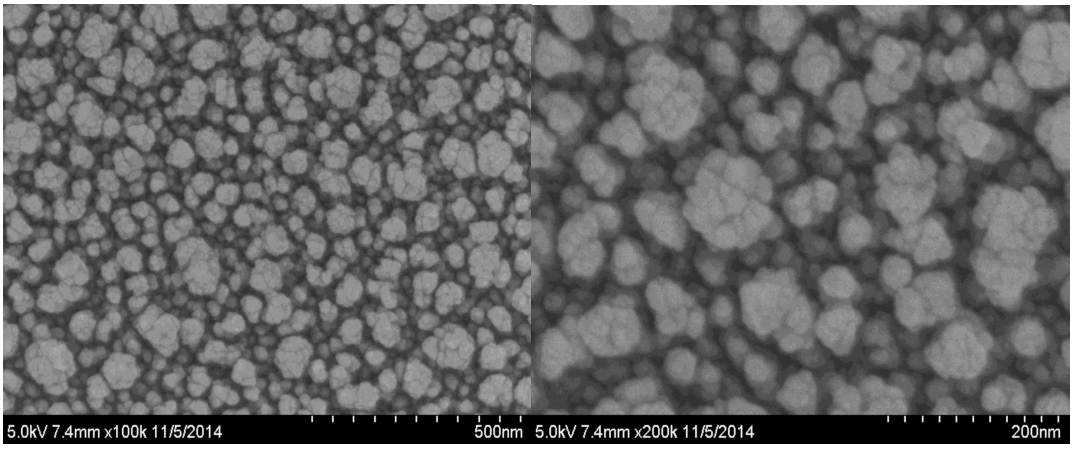

(a) Top view of S1 (b) Top view of S1

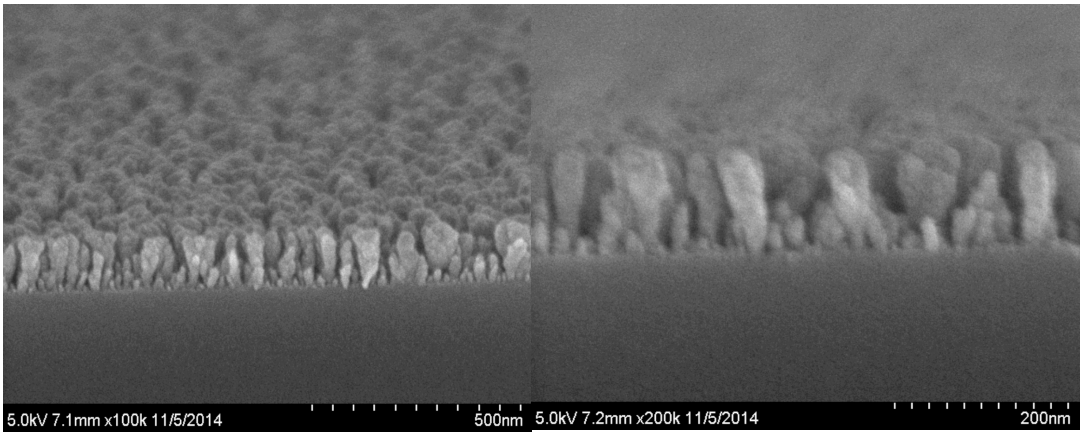

(c) cross sectional view of S1 (d) cross sectional view of S1

Figure 4.6: SEM images of the first sample of the hematite (a) and (b) are top view of the nanorods of hematite and (c) and (d) are the cross sectional view of the nanorods of the hematite.

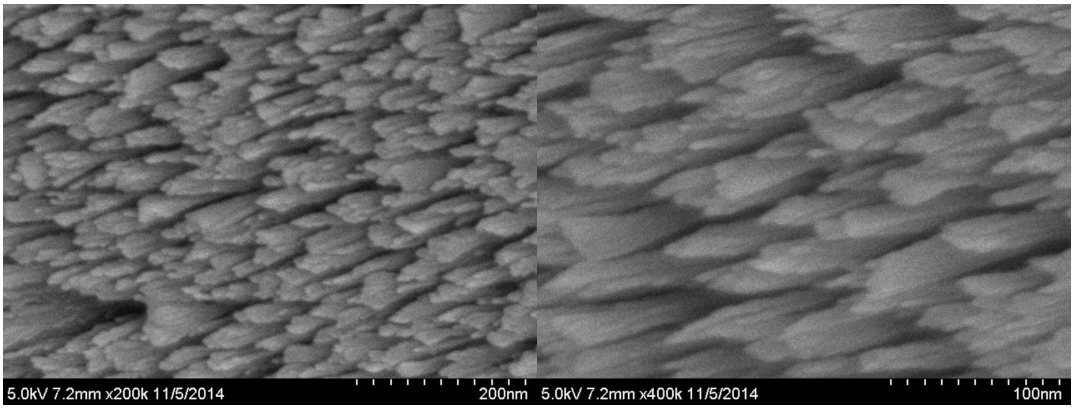

(a) Top view of S2 (b) Top view of S2

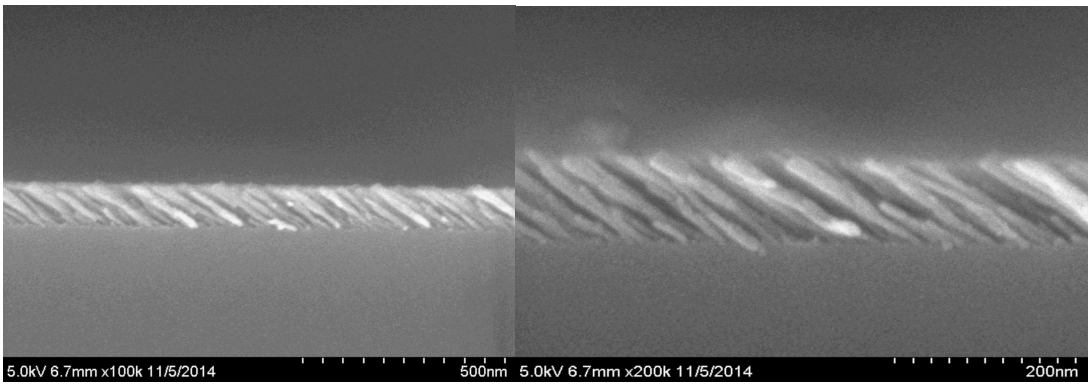

(c) Cross sectional view of S2 (d) Cross sectional view of S2

Figure 4.7: SEM images of the second sample of the hematite (a) and (b) are top view of the nanorods of hematite and (c) and (d) are the cross sectional view of the nanorods of the hematite.

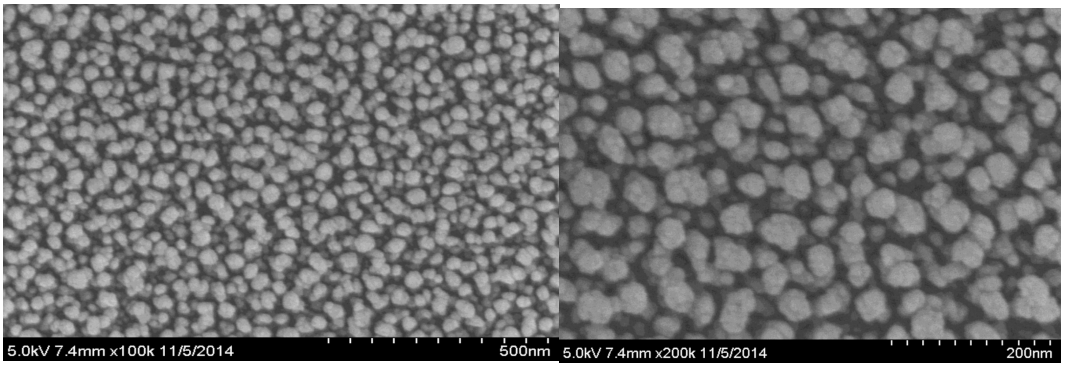

(a) Top view of S3 (b) Top view of S3

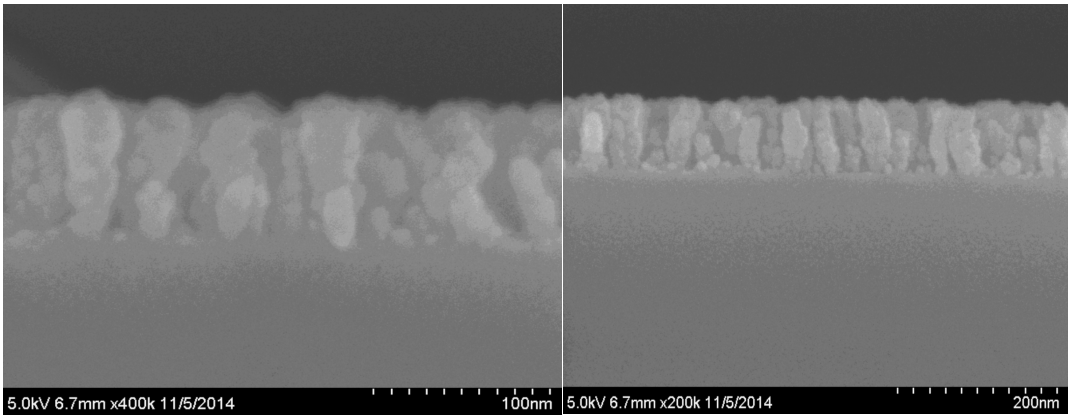

(c) Cross sectional view of S3 (d) Cross sectional of S3

Figure 4.8: SEM images of the third sample of the hematite (a) and (b) are top view of the nanorods of hematite and (c) and (d) are the cross sectional view of the nanorods of the hematite.

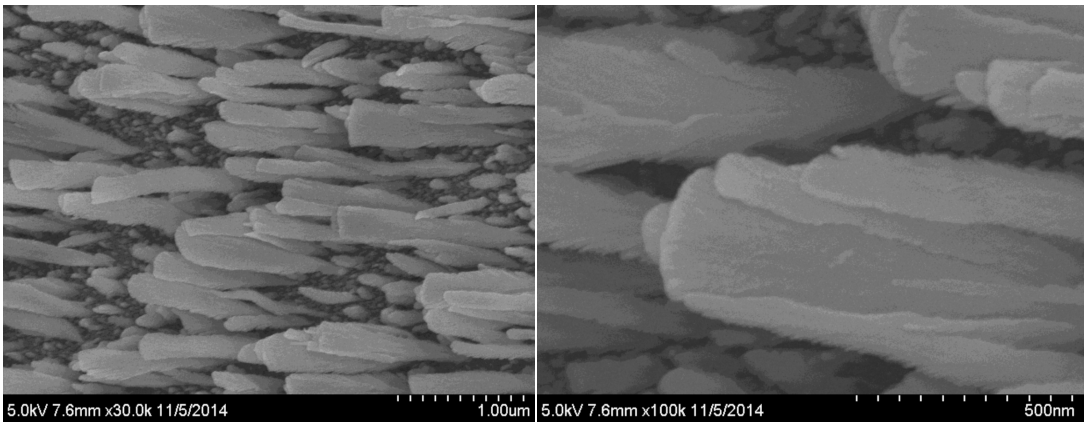

(a) Top view of S4 (b) Top view of S4

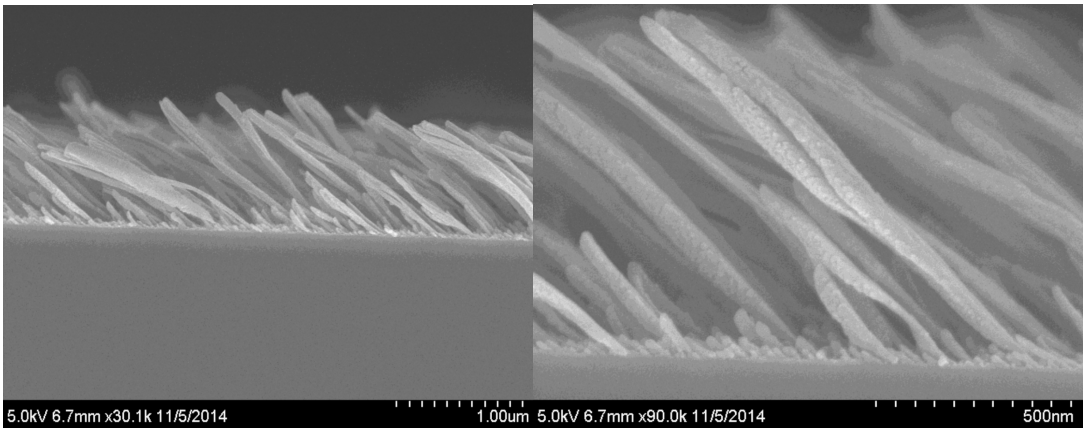

(c) Cross sectional view of S4 (d) Cross sectional of S4

Figure 4.9: SEM images of the sample of the magnetite (a) and (b) are top view of the nanorods of magnetite and (c) and (d) are the cross sectional view of the nanorods of the magnetite.

Chapter 5: Magnetic Properties

5.1 The vibrating sample magnetometer:

The vibrating sample magnetometer (VSM) is a scientific instrument that can be used to measure the magnetic moment or the magnetization of the material as a function of temperature and the applied magnetic field. It has been invented in 1955 by Simon Foner and then; in 1959, the paper about his work was published[27]. The principle of VSM depends on the electromagnetic induction phenomena when the sample undergoes a sinusoidal motion. The magnetic flux changes through the close area of the moving sample, resulting in the induced electrical signals (electromotive force) in a stationary pick-up coil[28 29 30]. The electromotive force is proportional to the magnetic moment of the sample. The principle of VSM can be ascribed by Faraday's law, as

$$\nu = -\frac{\partial \phi}{\partial t} \quad (5.1)$$

In 1959, Foner described VSM first and then many variants to the basic design of VSM have been made. All VSMs work by mounted the sample on the non-magnetic sample rod and then the sample vibrates between two pairs of coils by an oscillator As a result, change in magnetic flux produced in the coils, figure 5.1. The two pairs of coils are fixed and connected in order to collect the signal that caused by the moving of the sample and cancel any signal occurred due to the change in the field from the electromagnet. Since the magnetic induction by the sample at any point in the free space proportional to the magnetic moment of the sample:

$$\phi = gM \quad (5.2)$$

From equation 1 and 2, we can get that:

$v = -\frac{\partial gM}{\partial t}$ (5.3)

where g depends on the position of the sample which moves in the sinusoidal motion; so, the equation (5.3) will become:

$v = k\omega Aexp(i\omega t)M$ (5.4)

For the pick-up coils near R which maybe a electromechanical drive (voice coil) that is used to move the sample with a small vertical amplitude A and frequency ω the induced voltage will be*:*

$v_R = k_R\omega Aexp(i\omega t)M_R$ (5.5)

Where M_R is the constant of the magnetic moment of the reference; R and k_R is the coil geometry dependent constant.

The voltage that measured by the pick-up coils can be derive in a similar way:

$v_S = k_S\omega Aexp(i\omega t)M_S$ (5.6)

By taking the root-mean-square average of equations (5.5) and (5.6), the voltage induced in the detection coils will be known as:

$v_{OUT} = < v_S > rms / < v_R > rms = kM_S$ (5.7)

where k is the calibration constant that has taken in k_R, k_S and M_S .

From equation (5.7), it is seen that the voltage induced in the detection coils is

proportional to the magnetic moment of the sample since the frequency and the amplitude dependence is canceled.

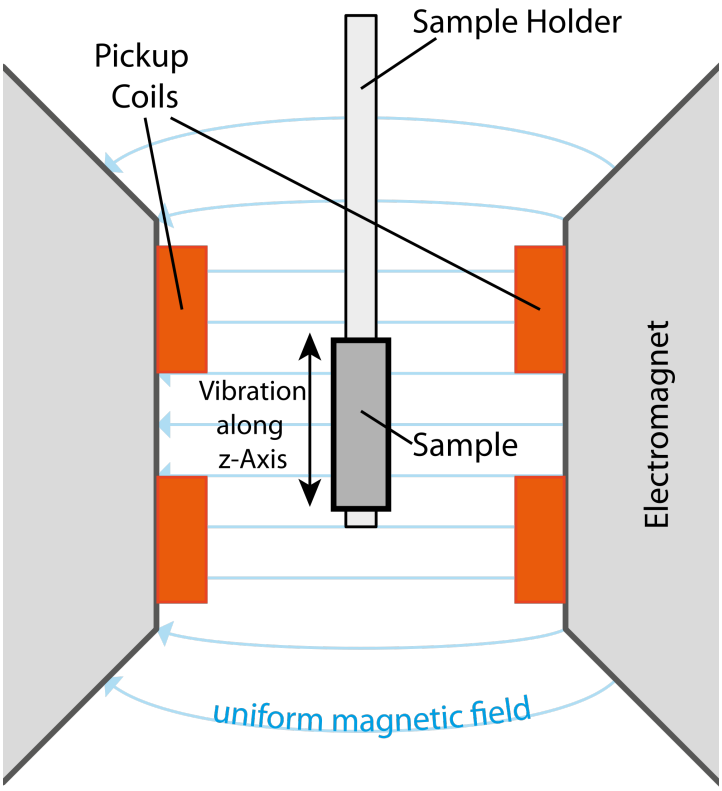

Figure 5.1: the sample holder and the detecting coils of vibrating sample magnetometer Credit: Wikipedia.

5.2 Study of the hysteresis Loop

By using VSM the response of substances to the application of external fields cyclically, the magnetic hysteresis was studied for all samples. The samples were subjected to an external applied magnetic field in cycles to obtain the hysteresis loops. For samples S1, S2 and S3 of hematite nanorods the field is first set up to 1200 Oe and

then decreased to -1200 Oe and then increased to the starting point again at 1200 Oe. By using the data of the field and the corresponding magnetic moment, the hysteresis loop will be obtained since the changing of the magnetic field will lead to the change in the magnetic moment of the samples. In the case of the magnetite sample, the magnetic field with a range between 3000 Oe and -3000 Oe has been applied because of the high saturation of the material. The orientation of the samples was adjusted to align the external magnetic field parallel or perpendicular to the surface plane of the substrates. The figures 5.2, 5.3, 5.4,and 5.5 show the hysteresis loops of S1, S2, S3 and S4 in perpendicular and parallel directions to the magnetic field.

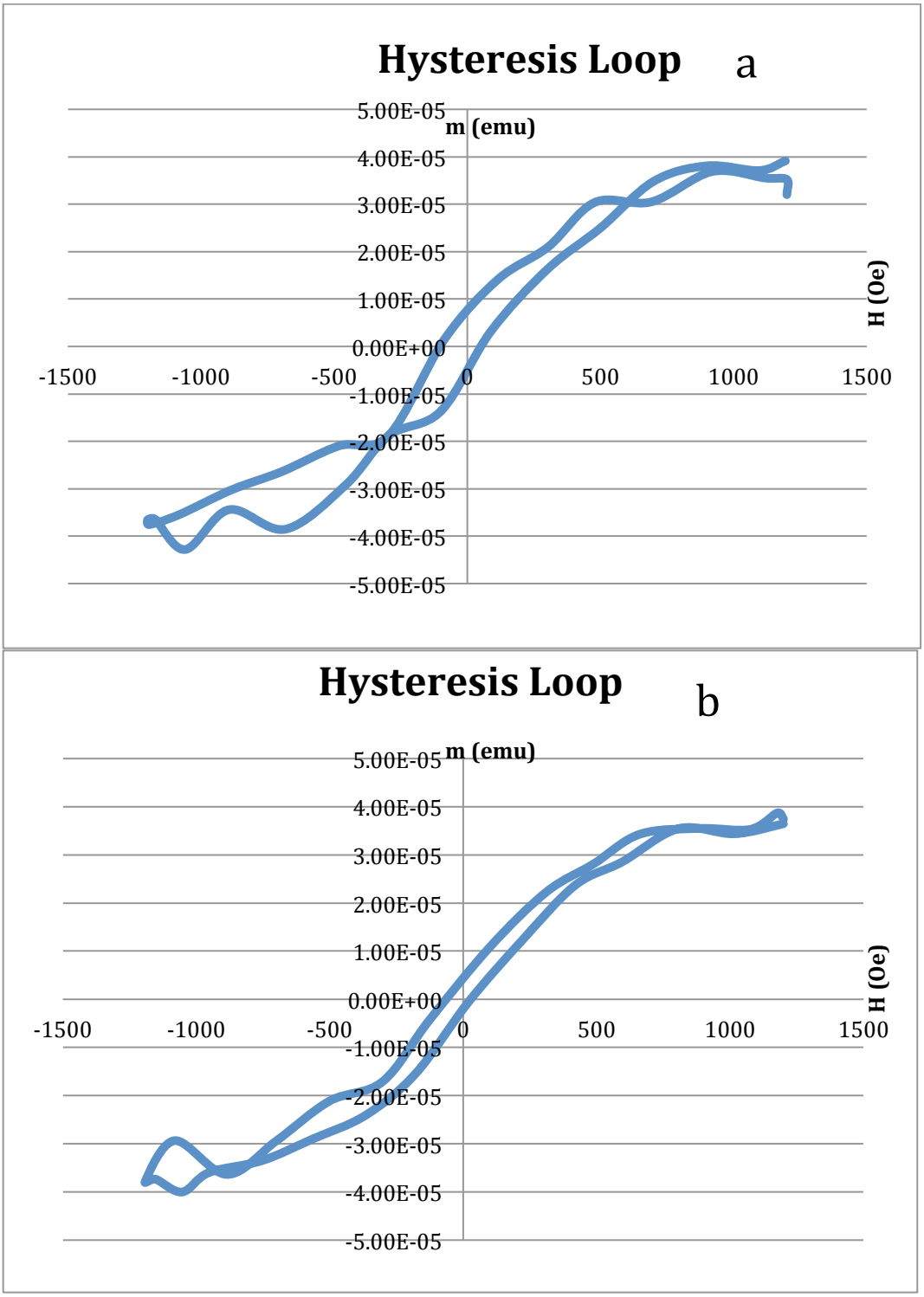

Figure 5.2: the hysteresis loop of the S1 with to direction with the magnetic field (a) Shows the loop when the nanorods are perpendicular to the magnetic field. (b) Shows the loop when the nanorods are parallel to the magnetic field.

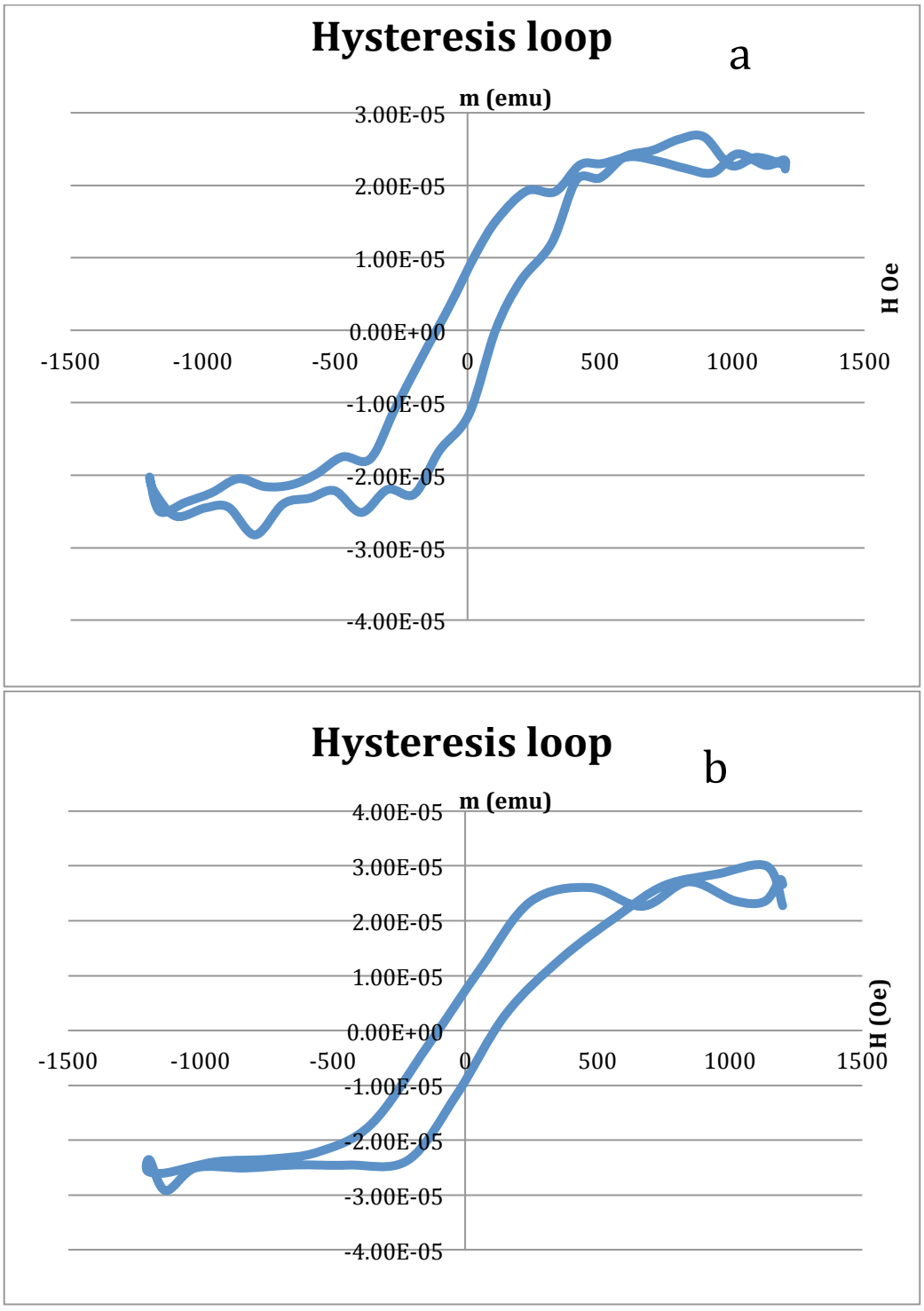

Figure 5.3: the hysteresis loop of the S2 with to direction with the magnetic field (a) Shows the loop when the nanorods are perpendicular to the magnetic field. (b) Shows the loop when the nanorods are parallel to the magnetic field.

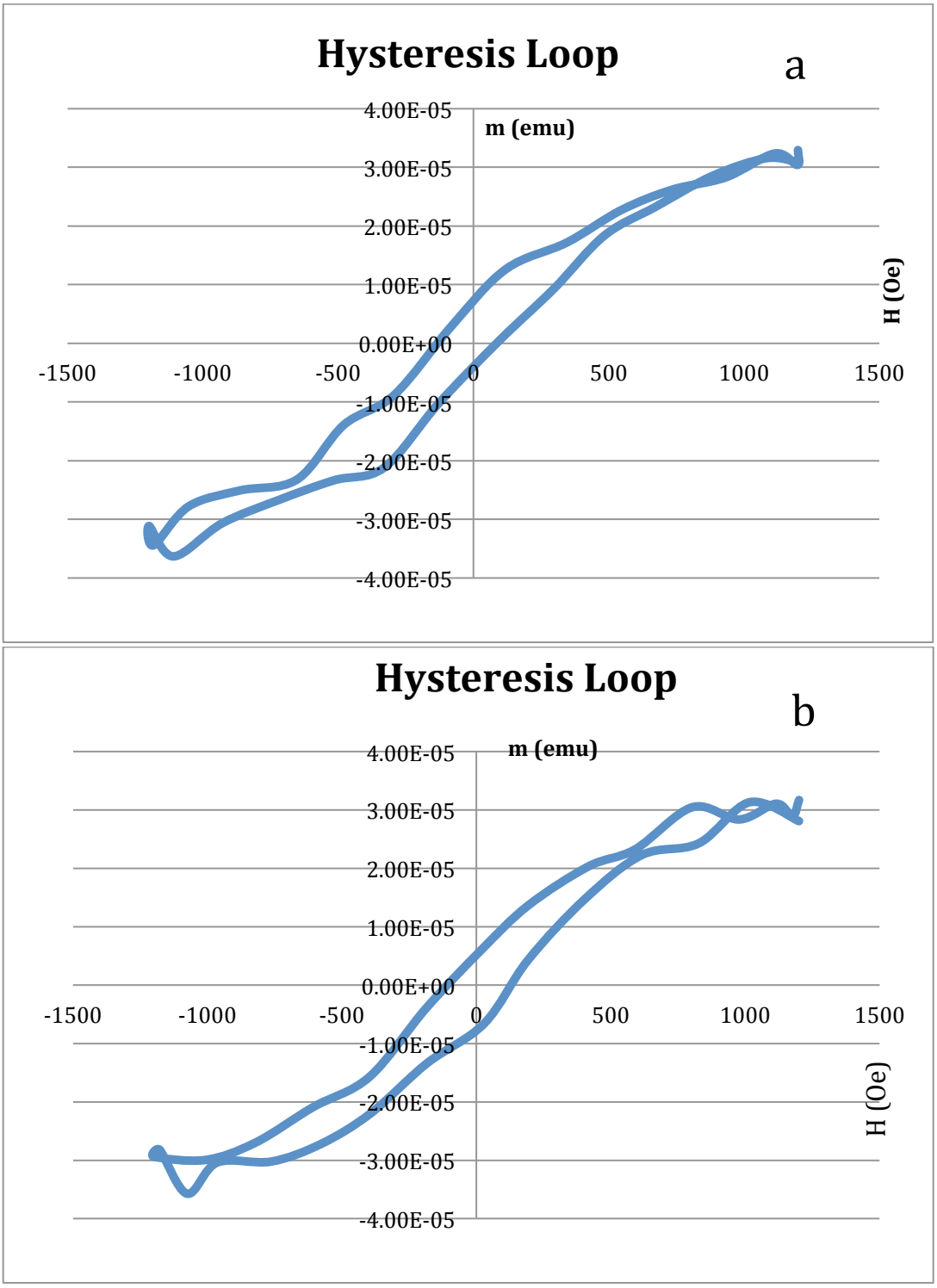

Figure 5.4: the hysteresis loop of the S3 with to direction with the magnetic field (a) Shows the loop when the nanorods are perpendicular to the magnetic field. (b) Shows the loop when the nanorods are parallel to the magnetic field.

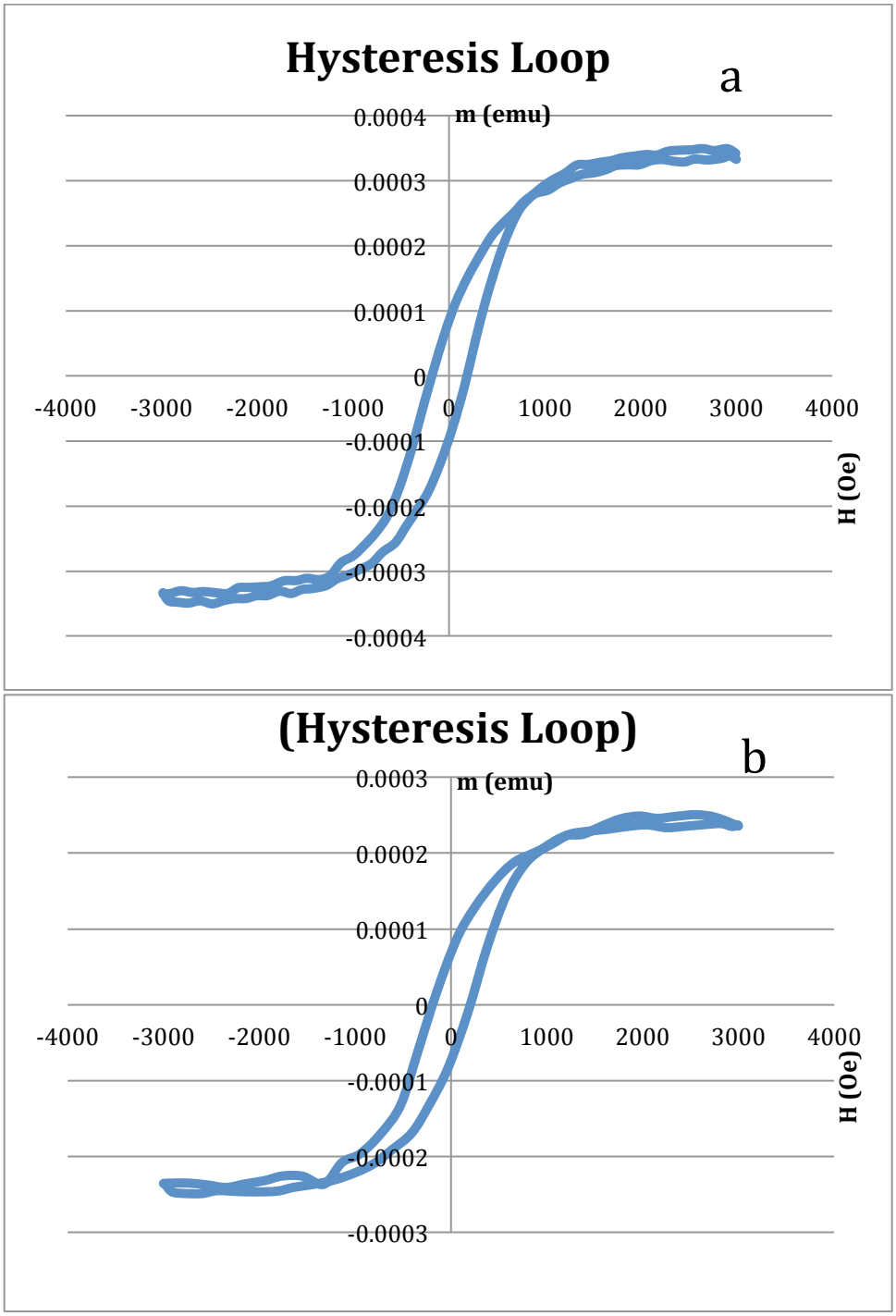

Figure 5.5: the hysteresis loop of the S4 with to direction with the magnetic field (a) Shows the loop when the nanorods are perpendicular to the magnetic field. (b) Shows the loop when the nanorods are parallel to the magnetic fie

Sample	M_S(emu)	M_R (emu)	H_C (Oe)
S1 Surface plane parallel to H	**$3.92\pm0.03\times10^{-5}$**	**$1.57\pm0.02\times10^{-5}$**	**100**
S1 Surface plane Perpendicular to H	**$3.84\pm0.01\times10^{-5}$**	**$0.42\pm0.03\times10^{-5}$**	**60**
S2 Surface plane parallel to H	**$2.73\pm0.02\times10^{-5}$**	**$1.16\pm0.01\times10^{-5}$**	**170**
S2 Surface plane Perpendicular to H	**$3.00\pm0.01\times10^{-5}$**	**$0.92\pm0.03\times10^{-5}$**	**165**
S3 Surface plane parallel to H	**$3.464\pm0.003\times10^{-5}$**	**$0.9810\pm0.03\times10^{-5}$**	**150**
S3 Surface plane Perpendicular to H	**$3.12\pm0.01\times10^{-5}$**	**$0.61\pm0.02\times10^{-5}$**	**120**
S4 Surface plane parallel to H	**$3.41\pm0.02\times10^{-4}$**	**$1.11\pm0.03\times10^{-4}$**	**167**
S4 Surface plane Perpendicular to H	**$2.50\pm0.03\times10^{-4}$**	**$8.70\pm0.01\times10^{-5}$**	**151**

Table 5.1: The value of saturation magnetization (M_S), remanence (M_R) and the coercivity (H_C) from the hysteresis loop of S1, S2, S3 and S4 in the two directions with the magnetic field.

The saturation magnetization M_S, remanence M_R, and coercivity H_C from the VSM measurements were listed in Table 5.1. From the table above it can be seen that the values M_R and H_C of all the samples mostly decreased when the Surface plane of the samples became perpendicular with respect to the magnetic field, but the rate of decline of the M_R and H_C values of the samples was different. The behavior of M_S, M_R and H_C of S1 and S3 are similar to each other when the Surface plane of the sample flips from parallel to perpendicular direction to the field. The values of M_R and H_C of S1 and S3 have decreased significantly when the Surface plane are turned 90° with respect to the

magnetic field. The table above indicates that M_S of sample S2 raised within the perpendicular direction with H, but the M_R and H_C are reduced Slightly with the perpendicular direction of the field. The values of M_S, M_R and H_C of S4 increased when the Surface plane of the sample becames parallel to the field. The behavior of the M_R and H_C of the S2 and S4 were similar when the nanorods are turned 90° with respect to the magnetic field. However the table shows that S4 has the largest value of the of M_S, M_R and H_C in the both direction with the field.

5.3 The temperature dependent magnetic properties:

In this work, using VSM, the low-temperature magnetic properties of hematite nanorods S2 has been studied. In order to understand the low-temperature magnetic properties of the hematite, the magnetic properties of the magnetite S4 has been studied and compared with the result of S2. The data were collected for the two samples from 50 to 300 K under ZFC and FC conditions. The figures blow show the curves for the temperature dependent magnetization (M-T) of ZFC and FC and the corresponding logarithmic ZFC and FC curves. Under an applied magnetic field of 100 Oe within perpendicular and parallel directions with the applying field, the T_M was determined. Since a small field sill applied in the ZFC condition which is less than 5 Oe, the curves for the temperature dependence magnetization of ZFC in the perpendicular and parallel directions have been studied for the S2 and S4, too. Figure 5.6 show the ZFC M-T curve of the S2 of hematite nanorods that are perpendicular to the < 5 Oe field and it indicates that the Block temperature (T_B) is about 102 K and no significant evidence of T_M. At the same direction with the field, FC M-T curve of the S2 of hematite nanorods displays in

the figure 5.7 (a) and it showed that the magnetization started to increase significantly at T_M which is around 100 K. As the direction of the S2 nanorods turned 90°, there were no observable change in the magnetization under the ZFC condition; however, under FC condition the behavior of the magnetization changed after 100 K and started to decrease slowly.

The results of the M-T curve of the S4 are remarkably different than the one we have get for the S2. Figures 5.10 and 5.11 show the ZFC and FC M-T curves when the nanorods of the sample are perpendicular to the field. From the figures 5.10 (a) and (b), it is very clear that the T_B is about 194 K, but when applied a 100 Oe magnetic field, the magnetization increased gradually from 66 K until 200 K and then stopped increasing, as it illustrated in the figure 5.11 (a). As the direction of the nanorods becomes parallel to the field, the T_B of the ZFC M-T curve shifted to 252 K, as can be seen in figures 6.12 (a) and (b). Figure 5.13 (a) shows the behavior of the magnetization as the temperature increased from 50 to 300 K and then decreased. At 250 K the magnetization increases again.

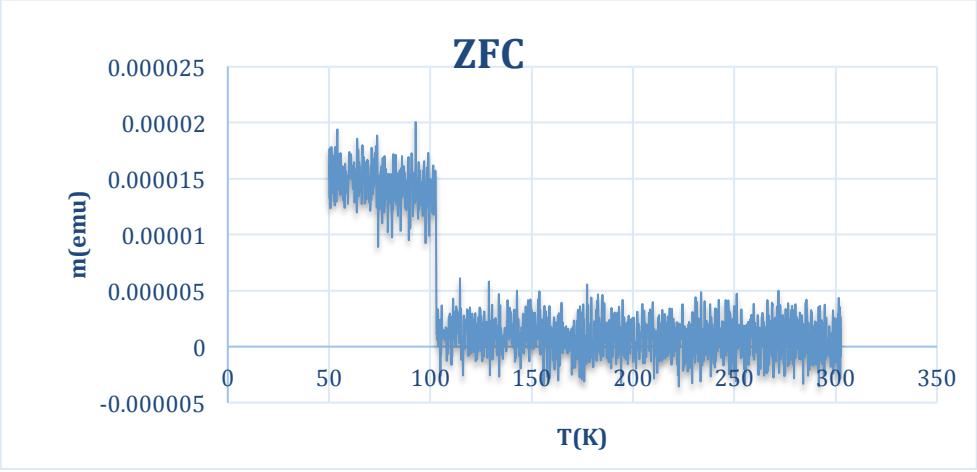

Figure 5.6: the Temperature dependence of ZFC magnetization for S2 in the perpendicular direction with the field.

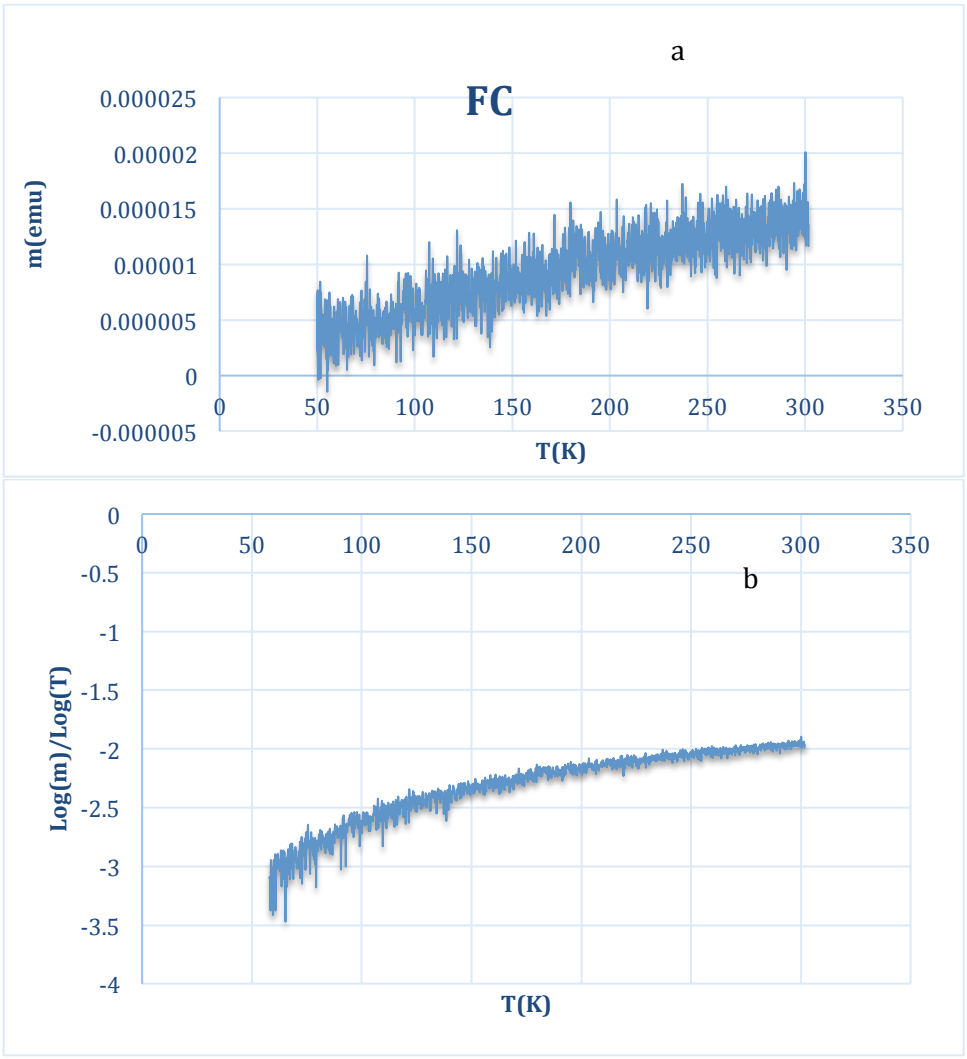

Figure 5.7: (a) the Temperature dependence of FC magnetization for S2 in the perpendicular direction to magnetic field (b) its corresponding logarithmic FC curves.

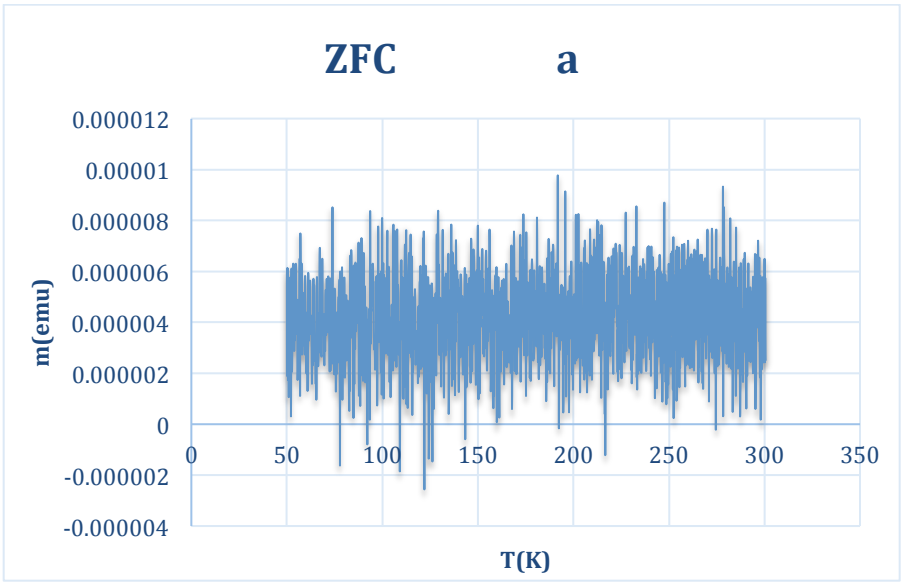

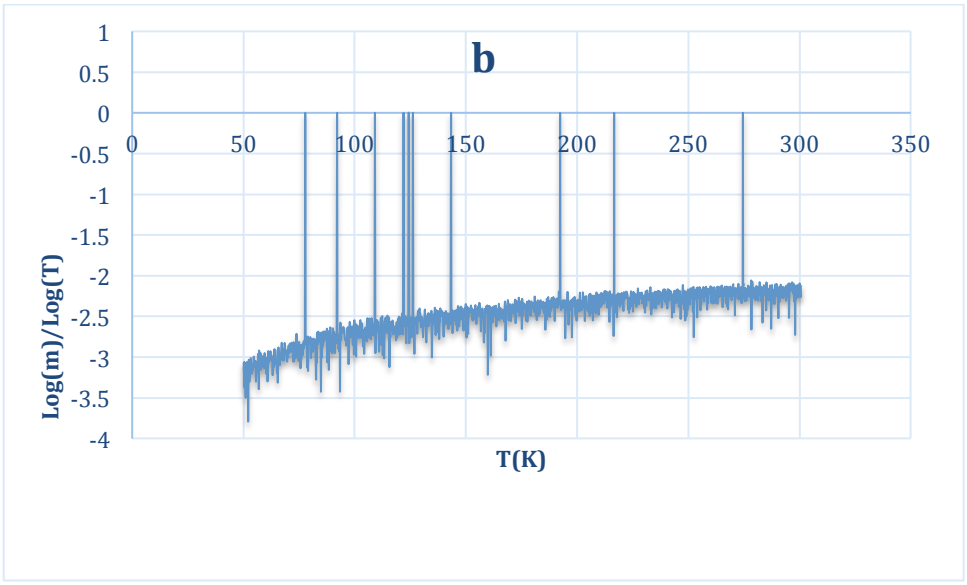

Figure 5.8: (a) the Temperature dependence of ZFC magnetization for S2 in the parallel direction with the field (b) its corresponding logarithmic ZFC curves.

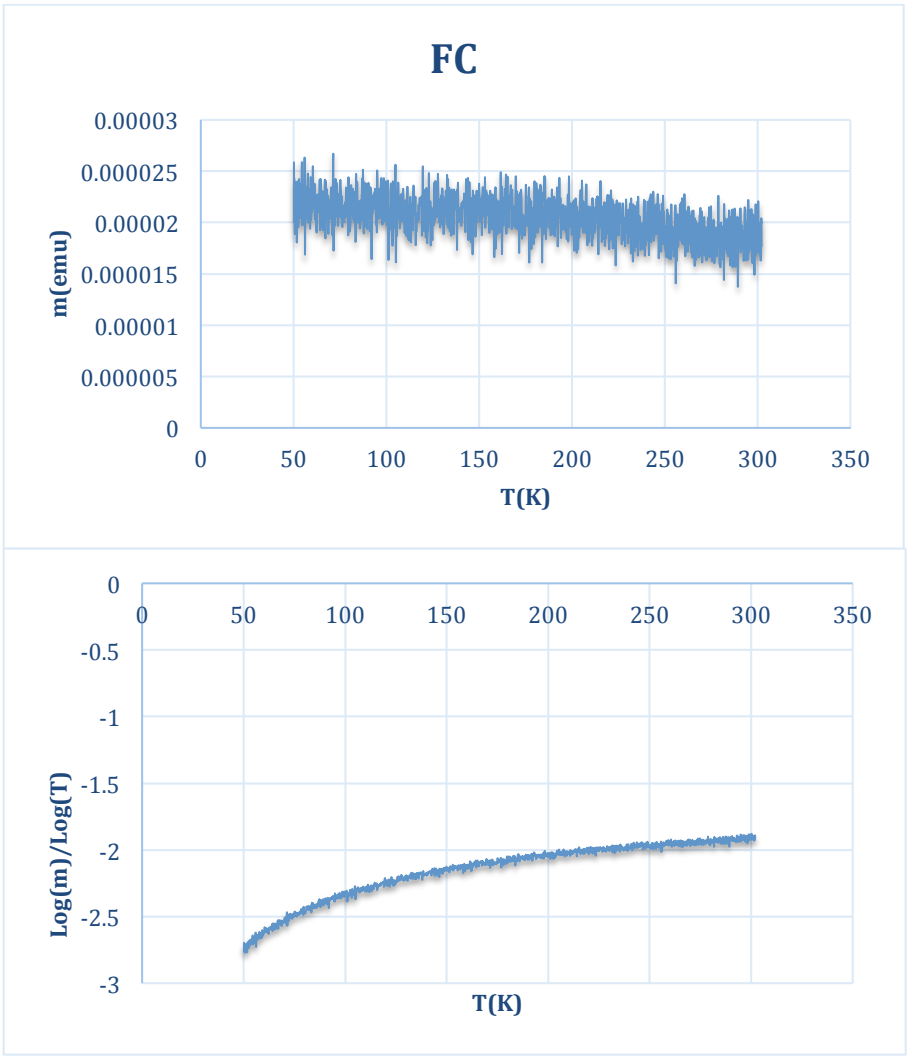

Figure 5.9: (a) the Temperature dependence of FC magnetization for S2 parallel to the magnetic field (b) its corresponding logarithmic FC curves.

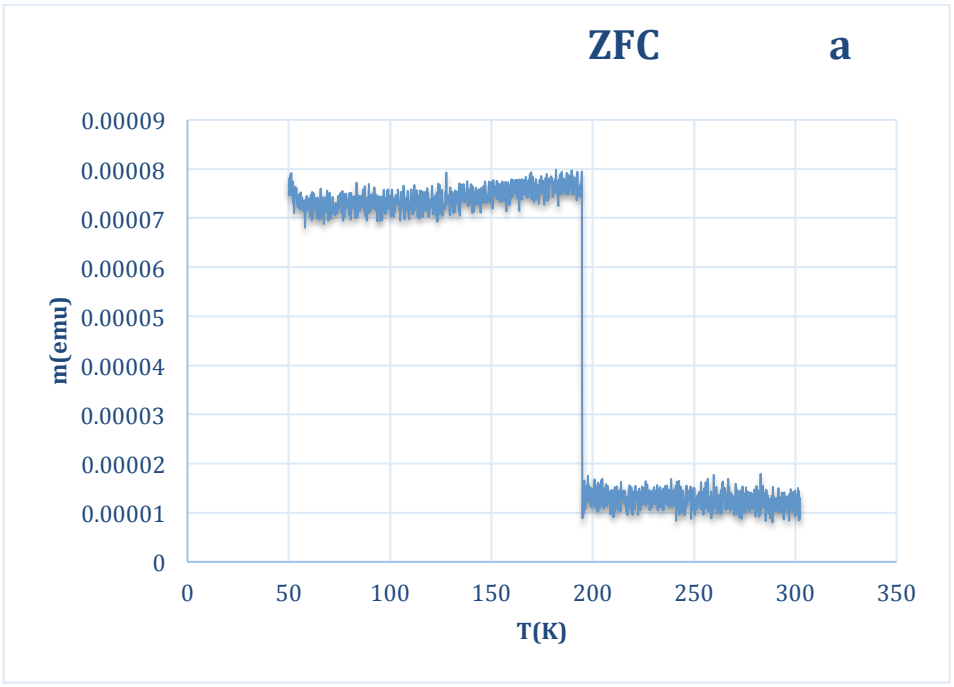

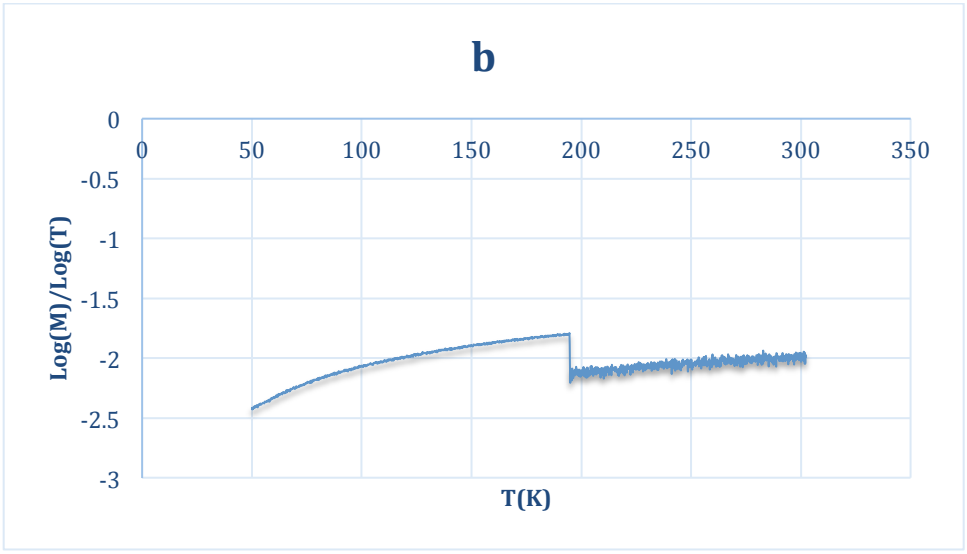

Figure 5.10: (a) the Temperature dependence of ZFC magnetization for S4 in the perpendicular direction to the field (b) its corresponding logarithmic FC curves.

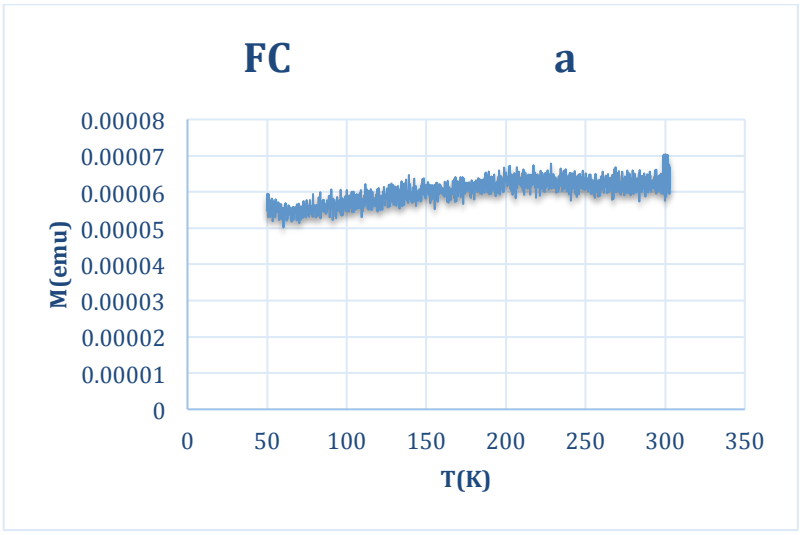

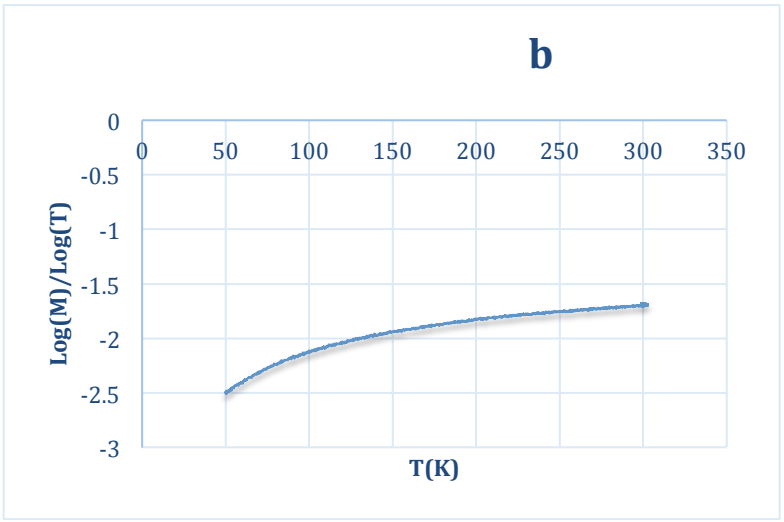

Figure 5.11: (a) the Temperature dependence of FC magnetization for S4 in the perpendicular direction to the field (b) its corresponding logarithmic FC curves.

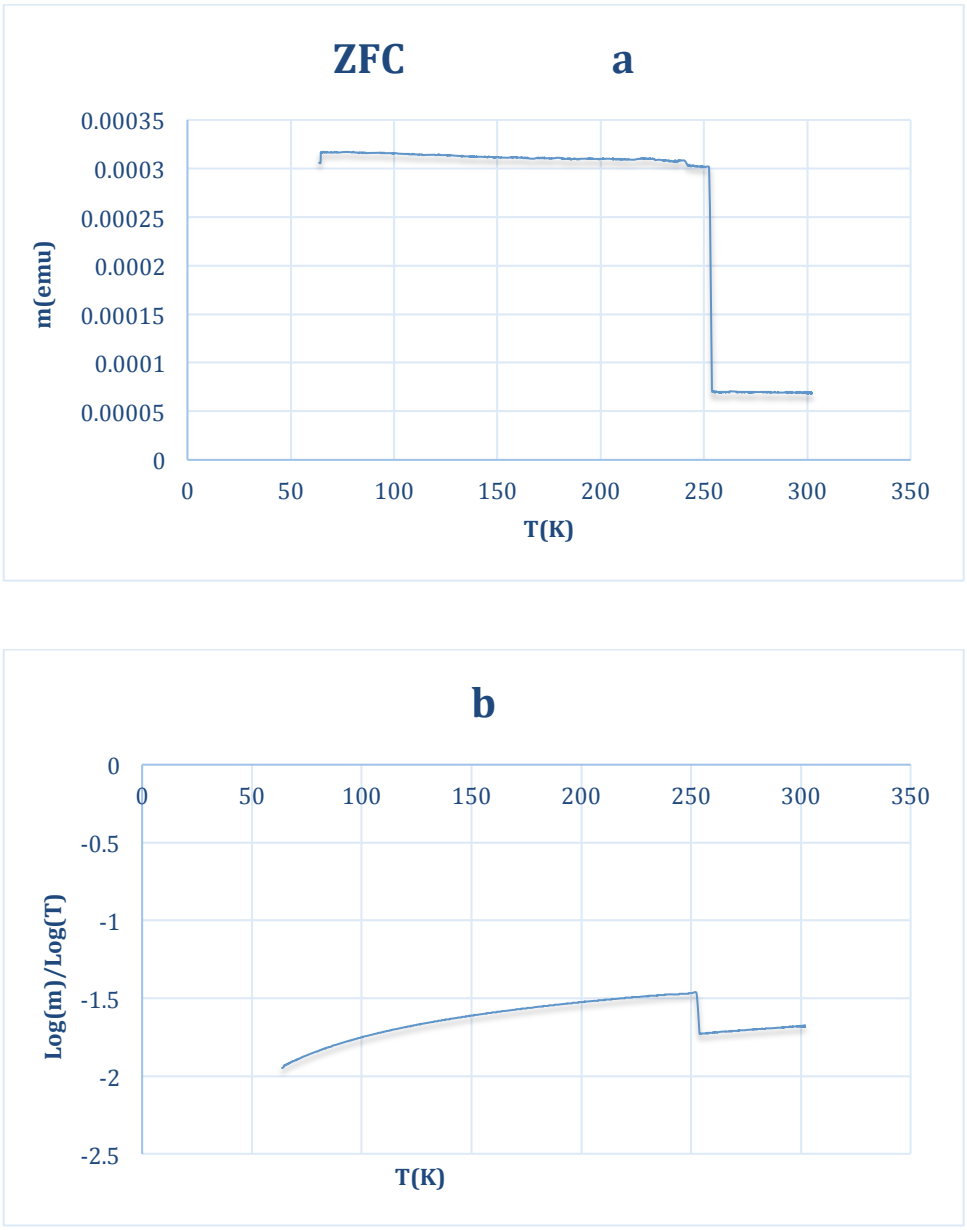

Figure 5.12: (a) the Temperature dependence of ZFC magnetization for S4 in the parallel direction to the field (b) its corresponding logarithmic FC curves.

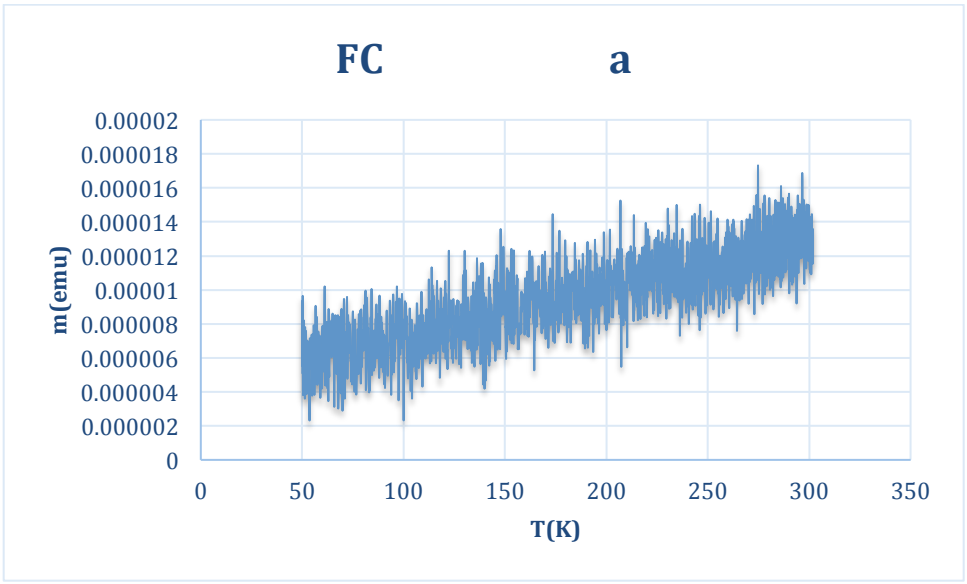

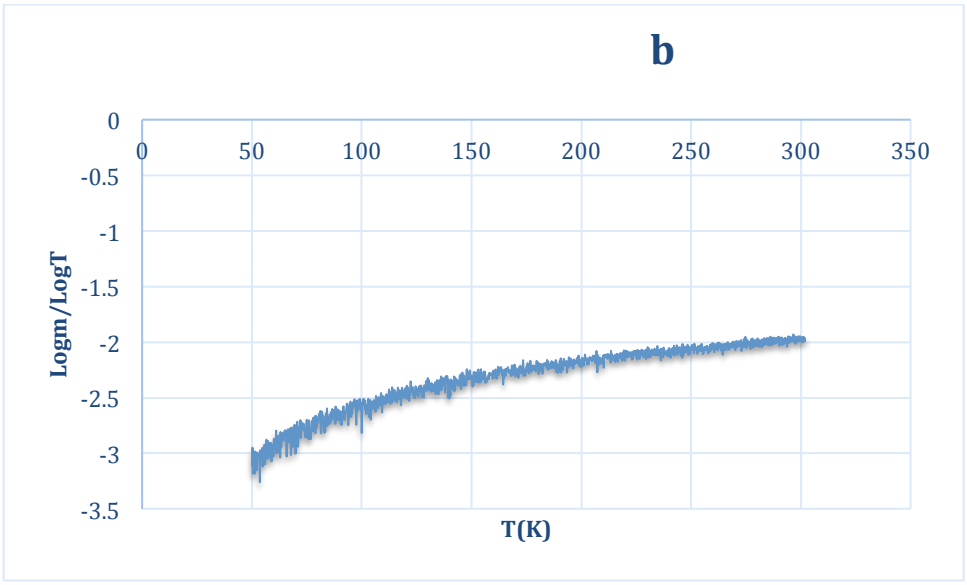

Figure 5.13: (a) the Temperature dependence of FC magnetization for S4 in the parallel direction to the field (b) its corresponding logarithmic FC curves.

5.4 The magnetic field direction dependence magnetic properties:

From the result that we have found in the 5.2 section, it can be seen that the hysteresis loop behaviors of S1 and S3 are similar and the hysteresis loop behaviors of S2 and S4 are similar as the direction of the nanorods change with the field. That can be explain better from the SEM images of the samples since it has found that S1and S3 has like morphology and S2 and S4 have like morphology. Therefore, the morphology has applied an important role in the magnetic properties of the nanorod. In addition, from the Table 5.1, it can be realized that the values of M_S, M_R, and H_C changed of all the samples by flipping the surface plane of the samples 90° to the magnetic field. Also, the table indicated that S2 and S4 has large hysteresis loops in both conditions, perpendicular or parallel direction to the field. That demonstrates the significant effect of direction of applied field to the nanorod on the magnetic properties, as it illustrated in the next figure. From the figures 5.14 (c) and (d), we can see that vertical nanorods may get less amount of the magnetic field when they are parallel to the field and that explains the huge decreasing in the M_R and H_C values of the S1 and S3 when their nanorods became parallel to the magnetic felid (H). However, the titled nanorods still get large amount of the field and that justifies the large hysteresis loops of the S2 and S4 samples even when they parallel to the field.

However, the studies of the temperature dependent magnetic properties of S2 with the two directions to the field showed different performance. When the nanorods of S2 were perpendicular to the field, The ZFC M-T curve showed that T_B is about the 102K

and FC M-T curve showed that the magnetization increased faster after 100K. But when the sample flipped 90° with the field, FC M-T curve displayed no T_B or T_M, but FC M-T curve showed that magnetization started to decrease at 100 K. Therefore, the M-T curves of S2 affected by the direction of the nanorod to field. From the figures 5.10, 5.11, 5.12, and 5.13, it has been found that the M-T curves of the S4 behaved differently when the direction of the nanorods changed from perpendicular to parallel with the field as well. Comparing the temperature dependence magnetic properties of S2 and S4 shows different M-T curves behavior of two of them.

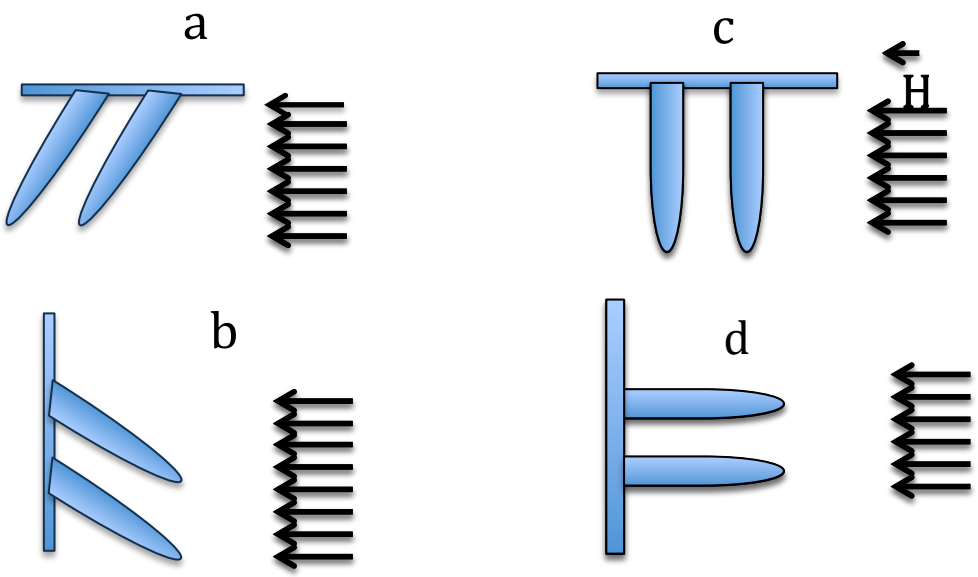

Figure 5.14: the a mount of the magnetic field that can pass throw the nanorod (a) when the nanorods are titled to the substrate and perpendicular (d)) when the nanorods are titled to the substrate and parallel to the field (c) when the nanorod are vertical to the substrate and perpendicular to the field (d) when the nanorod are vertical to the substrate and parallel to the field.

Chapter 6: Conclusions and Future Work

Three samples of hematite nanorod were deposited on the silicon substrates with different techniques. Sample S1 was prepared by using thermal deposition, partially ionized beam, and substrate rotation in glancing angle deposition technique. The second sample S2 was synthesized by using thermal deposition, partially ionized beam, and fixed substrate in glancing angle deposition. The sample S3 was obtained by using E beam deposition, partially ionized beam deposition, and rotating substrate in glancing angle deposition. One sample of magnetite was prepared to compare the magnetic properties between the two different iron oxide materials. The hysteresis loops of S1, S2, S3, S4 and the temperature dependent magnetic properties of S2 and S4 were studied.

Samples S1 and S3 have similar hysteresis loop behavior and the hysteresis loops of S2 and S4 are similar, too, as the direction of the nanorods changes with the field and that maybe due to the similarity of the morphology. In addition, samples S2 and S4 have large hysteresis loops in both conditions, perpendicular or parallel direction to the field. However, the values of M_S, M_R, and H_C of S4 are significantly larger than the the values of M_S, M_R, and H_C of the S2.

The studies of the temperature dependent magnetic properties of S2 and S4 showed that the Zero-field-Cooled (ZFC) and Field-Cooled (FC) magnetization - temperature (M-T) curves of S1and S4 behaved differently when the direction of the surface plane of the sample changed from perpendicular to parallel with the field. In addition, the ZFC and FC M-T curves of S2 were different than the ZFC and FC M-T

curves of S4. Therefore, the direction of the field to the surface plane of the sample is applied a remarkable affect on the magnetic properties of hematite and magnetite. Further work on this project could be studying the temperature dependent magnetic properties of the hematite sample that grow vertical to the substrate to compare the result to which we got from the titled nanorods.

References

[1] http://www.irm.umn.edu/hg2m/hg2m_b/hg2m_b.html#top

[2] http://www.irm.umn.edu/hg2m/hg2m_b/hg2m_b.html#top

[3] http://www.irm.umn.edu/hg2m/hg2m_b/hg2m_b.html#top

[4] Özdemir, Ö., D. J. Dunlop, and T. S. Berquo´ (2008), "Morin transition in hematite: Size dependence and thermal hysteresis", Geochem. Geophys. Geosyst., 9, Q10Z01 (2008), doi:10.1029/2008GC002110.

[5] http://en.wikipedia.org/wiki/Exchange_interaction

[6]http://research.pbsci.ucsc.edu/chemistry/li/teaching/chem268/Magnetic%20properties.pdf

[7] http://en.wikipedia.org/wiki/N%C3%A9el_temperature

[8] http://www.irm.umn.edu/hg2m/hg2m_b/hg2m_b.html#antiferromagnetism

[9] http://phys.thu.edu.tw/~hlhsiao/mse-web_ch20.pdf

[10] http://www.irm.umn.edu/hg2m/hg2m_d/hg2m_d.html

[11] http://magician.ucsd.edu/Essentials_2/WebBook2ch4.html

[12] Changzheng Wu, Ping Yin, Xi Zhu, Chuanzi OuYang, and Yi Xie*. "Synthesis of Hematite (r-Fe2O3) Nanorods: Diameter-Size and Shape Effects on Their Applications in Magnetism, Lithium Ion Battery, and Gas Sensors .", J. Phys. Chem. B 110, 17806–17812 Phys. Chem (2006).

[13] Shang-Bing Wang, Yu-Lin Min, and Shu-Hong Yu*. "Synthesis and Magnetic Properties of Uniform Hematite Nanocubes ." Physical Chemistry letters (2006).

[14] Marin Tadic´ a, ∗, Nada C˘itakovic´ b, Matjaz˘ Panjanc, Zoran Stojanovic´ d, Dragana Markovic´ a, Vojislav Spasojevic´ a., "Synthesis, morphology, microstructure and magnetic properties of hematite submicron particles .", J.ournal of Alloys and Comp.ounds 509, 7639 – 7644 (2011).

[15] Y.Y. Xu *, X.F. Rui, Y.Y. Fu, H. Zhang. , "Magnetic properties of a-Fe2O3 nanowires .", Chem.ical Phys.ics Lett.ers 410, 36 – 38 (2005).

[16] http://en.wikipedia.org/wiki/Polyvinylpyrrolidone

[17] Debasish Sarkar, a) Madhuri Mandal, and Kalyan Mandal,. "Domain controlled magnetic and electric properties of variable sized magnetite nano-hollow spheres .", JOURNAL J. OF Appl.PPLIED Phys.HYSICS 112, 064318 (2012).

[18] Jing Xu, Haibin Yang, Wuyou Fu, Kai Du, Yongming Sui, Jiuju Chen, Yi Zeng, Minghui Li, Guangtian Zou,. "Preparation and magnetic properties of magnetite nanoparticles by sol–gel method .", J.ournal of Magn. Magn. Mater. Magnetism and Magnetic Materials 309, 307 – 311 (2006).

[19] Yiwei Tan, Zhongbin Zhuang, Qing Peng, and Yadong Li*., "Room-Temperature Soft Magnetic Iron Oxide Nanocrystals: Synthesis, Characterization, and Size-Dependent Magnetic Properties .", Chem. Mater. 20, 5029 – 5034 (2008).

[20] Yimin Zhao, † Charles W. Dunnill,‡ Yanqiu Zhu,*,† Duncan H. Gregory,*,‡ Walter Kockenberger,§ Yanhui Li,† Weibing Hu,† Iftikhar Ahmad,† and David G. McCartney†., "Low-Temperature Magnetic Properties of Hematite Nanorods .", Chem. Mater. 19, 916 – 921 (2006).

[21] Tokuyama, Kiyoshi Miyake, And Takashi Tokuyama,. "Germanium And Silicon Ion Beam Deposition .", Thin solid Solid films Films 92, 123 – 129 (1982).

[22] Bernd Rauschenbach, Bernd. "Ion beam assisted deposition—a processing technique for preparing thin films for high-technology applications$.", science and directVacuum 69, 3 – 10 (2003).

[23] S. Mohan and M. Ghanashyam Krishna,. "OBJ A review of ion beam assisted deposition of optical thin films .", pergamon Vacuum 46, 645 – 659 (1994).

[24] Jens Bauer, 1 Michael Weise,1,a) Bernd Rauschenbach,1,b) Nadine Geyer,2 and Bodo Fuhrmann2., "Shape evolution in glancing angle deposition of arranged Germanium nanocolumns.", J. Appl. Phys. APPLIED PHYSICS 111, 104309 (2012).

[25] W. K. Choi1, 2, L. Li2, H. G. Chew,2 and F. Zheng1., "Synthesis and structural characterization of germanium nanowires from glancing angle deposition .", Nanotechnology 18, 385302 (2007).

[26] R. N. Tait, T. Smy, and M. J. Brett,. "structural Structural anisotropy in oblique incidence thin metal films .", J. Vac. Sci. Technolog. A 10, 1518 – 1521 vacuum science and technology A (1991).

[27] Simon Foner, Simon "versatile Versatile and sensitive vibrating-sample magnetometer",. Rev. Sci. Instrum. 30, 548 – 557 (1959).

[28] C.D. Graham., “hHigh-sensitivity magnetization measurements.”, Mater. Sci. Technol. 16, 97 – 101 (1999-2000).

[29] S. N. wWillcock, S. N. “An investigation of the magnetic properties of high tensile steels”. Thesis, University of Durham (1986).

[30] J.A. Gerber, W. L. Burmester, D. J. Sellmyer,W. a. “Simple Vibrating sample magnetometer.”, Rev. Sci. Instrum. 53, 691 – 693 AIP. (1982).